Title

Striatal Indirect Pathway Dysfunction Underlies Motor Deficits in a Mouse Model of Paroxysmal Dyskinesia.

Journal

Journal of Neuroscience, 42(13)

ISSN

0270-6474

Authors

Nelson, Alexandra B
Girasole, Allison E
Lee, Hsien-Yang
et al.

Publication Date

2022-03-30

DOI

10.1523/jneurosci.1614-20.2022

Peer reviewed

Neurobiology of Disease

Striatal Indirect Pathway Dysfunction Underlies Motor Deficits in a Mouse Model of Paroxysmal Dyskinesia

Alexandra B. Nelson,[1,2,4,5] Allison E. Girasole,[1,2,4,5] Hsien-Yang Lee,[2] Louis J. Ptáček,[1,2,4,5] and Anatol C. Kreitzer[1,2,3,4,5,6]

[1]UCSF Neuroscience Graduate Program, [2]Department of Neurology, UCSF, [3]Department of Physiology, UCSF, [4]Kavli Institute for Fundamental Neuroscience, [5]UCSF Weill Institute for Neurosciences, and [6]The Gladstone Institutes, San Francisco, California 94158

Abnormal involuntary movements, or dyskinesias, are seen in many neurologic diseases, including disorders where the brain appears grossly normal. This observation suggests that alterations in neural activity or connectivity may underlie dyskinesias. One influential model proposes that involuntary movements are driven by an imbalance in the activity of striatal direct and indirect pathway neurons (dMSNs and iMSNs, respectively). Indeed, in some animal models, there is evidence that dMSN hyperactivity contributes to dyskinesia. Given the many diseases associated with dyskinesia, it is unclear whether these findings generalize to all forms. Here, we used male and female mice in a mouse model of paroxysmal nonkinesigenic dyskinesia (PNKD) to assess whether involuntary movements are related to aberrant activity in the striatal direct and indirect pathways. In this model, as in the human disorder PNKD, animals experience dyskinetic attacks in response to caffeine or alcohol. Using optically identified striatal single-unit recordings in freely moving PNKD mice, we found a loss of iMSN firing during dyskinesia bouts. Further, chemogenetic inhibition of iMSNs triggered dyskinetic episodes in PNKD mice. Finally, we found that these decreases in iMSN firing are likely because of aberrant endocannabinoid-mediated suppression of glutamatergic inputs. These data show that striatal iMSN dysfunction contributes to the etiology of dyskinesia in PNKD, and suggest that indirect pathway hypoactivity may be a key mechanism for the generation of involuntary movements in other disorders.

Key words: **basal ganglia; dyskinesia; dystonia; endocannabinoid; striatum; synaptic plasticity**

Significance Statement

Involuntary movements, or dyskinesias, are part of many inherited and acquired neurologic syndromes. There are few effective treatments, most of which have significant side effects. Better understanding of which cells and patterns of activity cause dyskinetic movements might inform the development of new neuromodulatory treatments. In this study, we used a mouse model of an inherited human form of paroxysmal dyskinesia in combination with cell type-specific tools to monitor and manipulate striatal activity. We were able to narrow in on a specific group of neurons that causes dyskinesia in this model, and found alterations in a well-known form of plasticity in this cell type, endocannabinoid-dependent synaptic LTD. These findings point to new areas for therapeutic development.

Introduction

Abnormal involuntary movements, or dyskinesias, occur in a wide variety of neurologic disorders. These include neurodegenerative conditions, such as Huntington's disease, as well as disorders where the brain appears grossly normal, such as drug-induced disorders and many forms of dystonia. This finding suggests aberrant neural activity or connectivity may be the underlying basis for involuntary movements.

Several neural circuits have been implicated in dyskinesias, including the basal ganglia, cerebellum, thalamus, and cortex (Hendrix and Vitek, 2012; Shakkottai et al., 2017; Cenci et al., 2018). In dyskinesias associated with anatomic abnormalities, lesions are most commonly found in the basal ganglia (Sethi et al., 1987; Ohara et al., 2001) and cerebellum (Standaert, 2011). Basal ganglia deep brain stimulation is therapeutic in several

Received June 26, 2020; revised Jan. 20, 2022; accepted Feb. 7, 2022.

Author contributions: A.B.N., A.E.G., L.J.P., and A.C.K. designed research; A.B.N. and A.E.G. performed research; A.B.N. and A.E.G. analyzed data; A.B.N. wrote the first draft of the paper; A.B.N., A.E.G., L.J.P., and A.C.K. edited the paper; A.B.N. wrote the paper; H.-Y.L. contributed unpublished reagents/analytic tools.

This work was supported by National Institutes of Health K08 NS081001 to A.B.N., R01 R01NS101354 to A.B.N., R01 NS064984 to A.C.K., R01 NS078435 to A.C.K., and the William Bowes Neurogenetics Fund to L.J.P. A.B.N. is the Richard and Shirley Cahill Endowed Chair in Parkinson's Disease Research. A.E.G. was supported by the National Science Foundation Graduate Research Fellowship and the UCSF Discovery Fellows Program. We thank the UCSF NIAAA P50 Histology Core for sharing equipment; Philip Starr, Kevin Kelley, and Michael Oldham for valuable discussions; and Chloe Bair-Marshall and Matthew Lum for technical assistance.

The authors declare no competing financial interests.

Correspondence should be addressed to Alexandra B. Nelson at alexandra.nelson@ucsf.edu or Anatol C. Kreitzer at anatol.kreitzer@gladstone.ucsf.edu.

https://doi.org/10.1523/JNEUROSCI.1614-20.2022

forms of dyskinesia (Damier et al., 2007; Ramirez-Zamora and Ostrem, 2018), implying a role for basal ganglia circuitry. Moreover, abnormal activity has been found in conjunction with dyskinesias (including dystonia) in both the basal ganglia (Papa et al., 1999; Chiken et al., 2008; Liang et al., 2008; Schrock et al., 2009) and cerebellum (LeDoux et al., 1998; Calderon et al., 2011; Fremont et al., 2014; Washburn et al., 2019).

Few studies have established causal links between abnormal neural activity and dyskinetic movements. However, in some forms of dystonia, rodent studies suggest that aberrant cerebellar firing may cause involuntary movements; moreover, this activity can be propagated to the striatum via a disynaptic pathway (Calderon et al., 2011; Chen et al., 2014). In contrast, the striatum has been implicated in another condition, levodopa-induced dyskinesia (LID) (Alcacer et al., 2017; Hernández et al., 2017; Perez et al., 2017; Girasole et al., 2018; Ryan et al., 2018). It is unclear whether alterations in striatal firing are a general feature of dyskinesia or whether such changes are causal in other forms of disease. Thus, we investigated the role of striatal firing in an etiologically distinct mouse model of dyskinesia, paroxysmal nonkinesigenic dyskinesia (PNKD). PNKD is a rare human autosomal dominant disorder, in which patients experience dyskinetic attacks in response to caffeine, alcohol, or extreme stress. PNKD is associated with mutations in the gene *pnkd*, which has unknown function but is expressed in neurons and localizes to synapses (Y. Shen et al., 2011). The PNKD mouse model shows a robust phenotype of caffeine- and alcohol-induced dyskinetic attacks (Lee et al., 2012). Although neurochemical studies suggest that dopamine signaling may be altered, neither the neurophysiological signature of dyskinesia in PNKD nor its underlying cellular mechanisms have been identified.

A longstanding model of basal ganglia function posits that dyskinesia is associated with an imbalance in the activity of the striatal direct and indirect pathways (Albin et al., 1989; DeLong, 1990). This model hypothesizes that direct pathway activity promotes movement, whereas indirect pathway activity suppresses movement. A corollary is that increased firing of striatal direct pathway neurons (dMSNs), decreased firing of indirect pathway neurons (iMSNs), or both may contribute to dyskinesia. Indeed, recent pathway-specific recordings in LID show bidirectional changes in the activity of dMSNs and iMSNs (Parker et al., 2018; Ryan et al., 2018). Moreover, optogenetic and chemogenetic studies indicate that dMSN activation can recapitulate and/or worsen LID (Alcacer et al., 2017; Perez et al., 2017; Ryan et al., 2018), although reduced iMSN activity may also contribute (Alcacer et al., 2017). We hypothesized that similar changes in activity might contribute to dyskinesia in etiologically distinct but phenotypically similar PNKD.

To test whether striatal dMSNs and iMSNs show abnormal patterns of activity during dyskinesia in PNKD mice, we first performed single-unit recordings from optogenetically identified striatal projection neurons. These recordings in freely moving mice showed marked reductions in iMSN activity during dyskinetic attacks. Second, we used chemogenetic tools to bidirectionally modulate iMSN output, and found that decreased iMSN activity is required for dyskinetic attacks in PNKD mice. Finally, we used *ex vivo* electrophysiology to investigate the underlying cellular mechanisms, and identified endocannabinoid-dependent LTD of excitatory inputs onto iMSNs as a key contributor.

Materials and Methods

Animals. Hemizygous PNKD mice (Tg(RP24-112K19 Pnkd*/IRESDsRed), hereafter termed "PNKD mice"), were maintained on a C57Bl/6 background. For *in vivo* experiments, hemizygous PNKD mice were bred to WT C57Bl/6 (Jax), Adora2a-Cre (A2a-Cre), or Drd1-Cre (D1-cre line 217) hemizygous mice (Gong et al., 2003, 2007; Gerfen et al., 2013). PNKD-negative littermates were used as WT controls. For *ex vivo* slice physiology experiments, hemizygous PNKD mice were bred to hemizygous Drd1a-tdTomato or Drd2-GFP mice, to generate Drd1a-tdTomato or Drd2-GFP (WT control) and PNKD;Drd1a-tdTomato or PNKD;Drd2-GFP (PNKD) mice. Mice of either sex were used. All experiments were initiated in mice aged 2-4 months, terminating before the age of 6 months. We complied with local and national ethical and legal regulations regarding the use of mice in research. All experimental protocols were approved by the UCSF Institutional Animal Care and Use Committee.

Behavior. Mice were administered intraperitoneal (IP) saline and habituated to the open field (a clear acrylic cylinder, 25 cm diameter) for a minimum of 1 h daily for 2 d before experiments. Mice implanted with infusion cannulae were habituated to tethering and infusion (of saline) for a minimum of 2 d, to confirm that the infusion process alone did not trigger dyskinesia. In experiments involving chemogenetic manipulation of iMSNs in PNKD mice, both PNKD and WT control mice were habituated to saline injections 5 d/wk for ~2 weeks, to minimize the likelihood of a stress-induced dyskinetic attack in response to IP injection of a drug or its vehicle in subsequent experiments.

During experiments, mice were placed in the open field chamber and monitored by two cameras: one mounted directly above the chamber to capture overall locomotor activity, and another in front of the chamber to capture qualitative aspects of movement, particularly dyskinesia. Video-tracking software (Noldus Ethovision) was used to quantify movement. Manual scoring was performed live during experiments, using a slight modification of a previously published dyskinesia scale (Lee et al., 2012). In this modified scale, numerical ratings indicate the following behaviors: 1 (asleep, inactive); 2 (normal activity); 3 (increased activity); 4 (hyperactivity, running); 5 (jerky movement and slow patterned movement; repetitive exploration); 6 (fast patterned movement; repetitive exploration with hyperactivity); 7 (stereotyped movements; repetitive sniffing/rearing in one location); 8 (continuous purposeless gnawing, sniffing and/or licking); and 9 (chorea, observed as irregular purposeless jaw, tongue, or forepaw movements; dystonia). Two seizure episodes were observed after caffeine administration during the study and were excluded from the dataset. A score of 7 was used for animals with frequent, but not continuous, gnawing, sniffing, or licking movements. For chemogenetic and pharmacological experiments, dyskinesia was scored for 1 min every 5 min. For *in vivo* electrophysiology experiments, dyskinesia was scored for 1 min every 5 min, except for the period between drug injection and the onset of involuntary movements (here defined as a score of $\geq$7), when it was scored continuously in 1 min bins. In AM251 prophylaxis experiments, animals were randomized to the drug or vehicle, one of which was administered IP 30 min before administration of caffeine. On an interleaved experimental day, mice received the other treatment. JZL184 experiments were conducted in the same fashion. The experimenter was blinded to the drug being administered until after acquisition and analysis had been performed. Dyskinesia scores were averaged between 45 and 60 min and compared between vehicle and AM251 or JZL184 and vehicle groups.

Pharmacology. For *in vivo* experiments, animals were injected IP with saline (10 μl/g) or caffeine (Tocris Bioscience). Caffeine was dissolved in normal saline and injected IP at a final dose of 25 mg/kg in most experiments. In the experiments for Figure 8*F*, *G*, animals were administered caffeine at 2 or 10 mg/kg. Clozapine-N-oxide (CNO, Sigma) was dissolved in normal saline at 0.1 mg/ml and injected IP at a final dose of 1 mg/kg. AM251 (Tocris Bioscience) was dissolved in DMSO, diluted in a 1:1 solution of saline and polyethylene glycol, and injected IP at a final dose of 5 mg/kg. JZL-184 (Tocris Bioscience) was dissolved in DMSO, aliquoted, then diluted in normal saline and injected IP at a final dose of 16 mg/kg. For intracranial infusions, caffeine was dissolved in normal saline at a concentration of 100 mM.

For *ex vivo* slice experiments, picrotoxin (Sigma) was dissolved in warm water at 5 mM and added to ACSF for a final concentration of 50 μM. TTX (Abcam) was dissolved in water at a stock concentration of 1

mM and added to ACSF for a final concentration of 1 μM. WIN55212 was dissolved in DMSO at 10 mM and added to ACSF for a final concentration of 1 μM. CNO was dissolved in DMSO at 10 mM and then diluted in ACSF for a final concentration of 1 μM. Caffeine was dissolved in water and then diluted in ACSF for a final concentration of 1 μM.

Intracranial infusion. Two- to 4-month-old mice were implanted with bilateral infusion cannulae. Anesthesia was induced with IP ketamine/xylazine and maintained with inhaled isoflurane. After opening the scalp, two small holes were drilled over the dorsolateral striatum (DLS; 0.8 AP, 2.2 mm DV from bregma) on either side of the skull using a stereotax-mounted drill. The exposed skull surface was scored with a scalpel to maximize adhesion of dental cement. Dental cement (Metabond) was applied to the exposed skull surface and the double-infusion cannula (PlasticsOne). The infusion cannula (with inner dummy cannula with cap screwed into place) was then lowered into the brain, with the tip of the inner cannula lowered to −2 mm DV from the brain surface. The cannula was then secured to the skull by application of dental acrylic (Ortho-Jet). After the acrylic had set, the scalp was closed with suture, and the mouse was allowed to recover from anesthesia. Buprenorphine (IP, 0.05 mg/kg) and ketoprofen (subcutaneous injection, 5 mg/kg) were administered for postoperative analgesia.

Behavioral experiments began 1 week following surgery. The experimenter was blinded to the genotype of the animal. In each session, the dummy inner cannula was removed, and a drug infusion inner cannula was placed inside the outer cannula, and screwed into place. The mouse was then returned to its home cage with the top removed, so it could move freely during drug infusion. Drug or saline was infused bilaterally using a Hamilton double syringe pump (WPI) at a rate of 0.1 μl per minute for a total volume of 0.5 μl per side. The cannula was left in place for an additional 3 min, after which both infusion cannulae were removed. The mouse was then transferred to the open field behavioral chamber for simultaneous video-tracking (for locomotion) and manual scoring (for dyskinesia). Infusion experiments were performed a minimum of 24 h apart.

To verify cannula function and to mark the location and estimate the extent of drug infusions, a lipophilic fluorescent dye was infused before sacrifice. After the final infusion experiments, 0.5 μl of the dye (FM4-64×, Thermo Fisher Scientific) was infused in the same fashion, after which terminal anesthesia was administered and transcardial fixative perfusion was performed. Tissue was processed and imaged to validate infusions (data not shown).

In vivo *electrophysiology/optogenetics.* To construct optrode arrays, optical fiber-ferrule assemblies were cemented onto 32 channel microelectrode arrays (Innovative Neurophysiology). Optical fiber-ferrule assemblies consisted of a 200 μm optical fiber (Thorlabs) threaded through a ceramic ferrule (Thorlabs) and cemented with epoxy. The tip of the optical fiber was positioned in the center of the array, ~0.5 mm above the tips of the microelectrodes. Surgical implantation of optrode arrays was performed at 2-4 months of age. Anesthesia was induced with IP ketamine/xylazine and maintained with inhaled isoflurane. Mice were stereotaxically injected with AAV5-DIO-ChR2-eYFP (UPenn Vector Core, 1 μl of 1:1 diluted virus) in the left DLS (0.8 AP, 2.25 ML, and −2.5 mm DV from bregma) through a small hole in the skull. Using a stereotax-mounted drill, this hole was later enlarged into a rectangular craniectomy and the dura was removed to permit implantation of the optrode. Small holes were also made in the right frontal and right posterior areas for later insertion of a skull screw (Fine Scientific Tools) and the ground wire, respectively. The exposed skull surface was scored with a scalpel to maximize adhesion of dental cement. Dental cement (Metabond) was applied to the exposed skull surface and the base of the optrode array connector. The optrode array was then slowly lowered into the center of the craniectomy to a depth of 2.3-2.4 mm from the brain surface. The array, ground wire, and skull screw were secured to the skull by application of dental acrylic (Ortho-Jet). After the acrylic had set, the scalp was closed with suture, and the mouse was allowed to recover from anesthesia. Buprenorphine (IP injection, 0.05 mg/kg) and ketoprofen (subcutaneous injection, 5 mg/kg) were administered for postoperative analgesia.

Two weeks after implantation, mice were habituated to tethering, the recording chamber, and IP saline injection for a minimum of 1 h daily for 2 d. After habituation, experimental sessions occurred approximately twice weekly for 2-6 weeks. During each session, electrical signals (single-unit and local field potential data from each of the 32 channels) were collected using a multiplexed 32 channel headstage (Triangle Biosystems), an electrical commutator equipped with a fluid bore (Dragonfly), filtered, amplified, and recorded on a MAP system, using RASPUTIN 2.4 HLK3 acquisition software (Plexon).

During recording sessions, after a baseline period, caffeine was injected IP. If a mouse developed stress-induced dyskinesia after tethering, but before drug administration, the experiment was terminated. After a period of 2-6 h of recording spontaneous activity in the open field, an optogenetic cell identification protocol was applied (Kravitz et al., 2013), consisting of 100 ms blue light pulses, given at 1 Hz. At each of four light powers (0.5, 1, 2, and 4 mW typically), 1000 light pulses were delivered via a lightweight patch cable (Doric Lenses) connected to a blue laser (Shanghai Laser and Optics Century), via an optical commutator (Doric Lenses), and controlled by TTL pulses from a behavioral monitoring system (Noldus Ethovision). At the end of this cell identification protocol, the animal was detached from the electrical and optical cables and returned to its home cage.

Single units were identified offline by manual sorting using Offline Sorter 3.3.5 (Plexon) and principal components analysis. Clusters were considered to represent a single unit if (1) the unit's waveforms were statistically different from multiunit activity and any other single units on the same wire, in 3D principal components analysis space, and (2) no interspike interval <1 ms was observed. Single units were classified as putative MSNs based on waveform and interspike interval distribution, using previously published criteria (Gage et al., 2010) to exclude fast-spiking interneurons.

After single units had been selected for further study, their firing activity was analyzed using NeuroExplorer 4.133 (Nex Technologies). To determine whether a unit was optogenetically identified, a peristimulus time histogram was constructed around the onset of laser pulses. To be considered optogenetically identified, a unit had to fulfill three criteria: (1) firing rate increased above the 99% CI of the baseline within 15 ms of laser onset; (2) firing rate was above this threshold for at least 20 ms; and (3) laser-activated waveforms were not statistically distinguishable from spontaneous waveforms. For display and analysis purposes, the firing rate of single units was averaged in 1 min bins.

Chemogenetics. AAVs encoding Cre-dependent constructs were stereotaxically injected 2-4 weeks before the first behavioral or slice physiology experiments. Littermates were randomized to DREADD or control fluorophore groups. For chemogenetic inhibition of iMSNs, A2a-Cre mice (either WT or PNKD) were stereotaxically injected with either AAV5-DIO-hM4D(G_i)-mCherry or AAV5-DIO-mCherry (UNC Vector Core, 1 μl) at four sites to cover the bilateral DLS (±1.0 AP, ±2.2 ML, −2.5 mm DV). For chemogenetic activation of iMSNs, PNKD;A2a-Cre mice were injected with either AAV5-DIO-hM3D(G_s)-mCherry or AAV5-DIO-mCherry (UNC Vector Core, 1 μl) at 8 sites per side to cover the majority of the striatum, bilaterally (0.8 AP, ±2.2 ML, −2.5, −4.0 DV; 0.8 AP, ±1.2 ML, −2.5, −4.0 DV; 0.0 AP, ±2.0 ML, −2.5, −3.7 DV; −0.5 AP, ±2.5 ML, −2.0, −3.0 DV). After a recovery period, mice were then habituated daily to the behavioral chamber and to IP injection of saline, to reduce the chance of stress-induced dyskinetic attacks when later injected with an experimental agent.

During chemogenetic inhibition experiments, on interleaved days, mice were injected IP with either saline or CNO, after which their behavior was monitored with both video-tracking of locomotor activity and manual scoring of dyskinesia (see Behavior, above). During chemogenetic activation experiments, on interleaved days mice were injected IP with either saline or CNO 20 min before injection of caffeine, and behavior was monitored. The experimenter was blinded to the viral construct injected in the mice.

Slice electrophysiology. For recordings in the dyskinetic state, animals (1.5-4 months old) were handled, then placed in a 500 ml glass beaker for 5 min before preparation of brain slices. In PNKD mice, such handling in unhabituated animals produced stress-induced dyskinetic attacks, as has been previously described (Lee et al., 2012). For recordings in the nondyskinetic state, PNKD animals were habituated to daily

handling and IP injections of saline to reduce the chance that terminal procedures would elicit a stress-induced attack. Mice were then deeply anesthetized with an IP ketamine-xylazine injection, transcardially perfused with ice-cold sucrose- or glycerol-based slicing solution, decapitated, and the brain was removed and placed in the slicing chamber with ice-cold slicing solution. Sucrose slicing solution contained the following (in mM): 79 NaCl, 23 $NaHCO_3$, 68 sucrose, 12 glucose, 2.3 KCl, 1.1 NaH_2PO_4, 6 $MgCl_2$, and 0.5 $CaCl_2$. Glycerol slicing solution contained the following (in mM): 250 glycerol, 2.5 KCl, 1.2 NaH_2PO_4, 10 HEPES, 21 $NaHCO_3$, 5 glucose, 2 $MgCl_2$, 2 $CaCl_2$. The brain was mounted on a submerged chuck, and sequential 300 μm coronal slices were cut on a vibrating microtome (Leica), transferred to a chamber of warm (34°C) carbogenated ACSF containing the following (in mM): 125 NaCl, 26 $NaHCO_3$, 2.5 KCl, 1 $MgCl_2$, 2 $CaCl_2$, 1.25 NaH_2PO_4, 12.5 glucose for 30-60 min, then stored in carbogenated ACSF at room temperature. Each slice was then submerged in a chamber superfused with carbogenated ACSF at 31°C-33°C for recordings.

MSNs were targeted for recordings using differential interference contrast optics in Drd1a-tdTomato or D2-GFP mice. In Drd1a-tdTomato mice, direct pathway neurons were identified by their tdTomato-positive somata, and indirect pathway neurons were identified by their tdTomato-negative medium-sized somata. In D2-GFP mice, indirect pathway neurons were identified by their GFP-positive somata, and direct pathway cells were identified by their GFP-negative medium-sized somata. Fluorescence-negative neurons with GABAergic interneuron physiological properties (membrane tau decay $<$1 ms for both fast-spiking and persistent low-threshold spiking subtypes; input resistance $>$500 MΩ in persistent low-threshold spiking subtype) were excluded from the analysis. Neurons were patched in whole-cell current-clamp or voltage-clamp configurations using borosilicate glass electrodes (3-5 MΩ) filled with either potassium-based (current-clamp) or cesium-based (voltage-clamp) internal solution containing the following (in mM), respectively: 130 $KMeSO_3$, 10 NaCl, 2 $MgCl_2$, 0.16 $CaCl_2$, 0.5 EGTA, 10 HEPES, 2 MgATP, 0.3 NaGTP or 120 $CsMeSO_3$, 15 CsCl, 8 NaCl, 0.5 EGTA, 10 HEPES, 2 MgATP, 0.3 NaGTP, 5 QX-314, pH 7.3. Picrotoxin was added to the external solution to block synaptic currents mediated by $GABA_A$ receptors. Drugs were prepared as stock solutions and added to the ACSF to yield the final concentration.

Whole-cell recordings were made using a MultiClamp 700B amplifier (Molecular Devices) and ITC-18 A/D board (HEKA). Data were acquired using Igor Pro 6.0 software (Wavemetrics) and custom acquisition routines (mafPC, courtesy of M. A. Xu-Friedman). Whole-cell recordings were filtered at 2 kHz and digitized at 10 kHz. All recorded neurons exhibited electrophysiological characteristics of MSNs. In current-clamp recordings to measure intrinsic properties, membrane potential (V_m) was measured as the average V_m 5-10 min after break-in. A series of small negative current steps were delivered from rest to calculate the input resistance of each cell. Rheobase and other input-output properties were obtained by giving a series of square-wave current steps, ranging from 100 to 800 pA (or the maximum current at which a cell could sustain spiking across the step), in 100 pA increments, with a 10 s interstimulus interval. Synaptic currents were monitored at a holding potential of −70 mV. Series resistance and leak currents were monitored continuously. Miniature EPSCs (mEPSCs) were recorded at –70 mV in TTX and picrotoxin. The mEPSC amplitude threshold was set at 5 pA. Only cells with at least 500 mEPSC events were included in the analysis. Cumulative probability plots were generated from 500 randomly selected mEPSC events. Evoked EPSCs onto MSNs were elicited in the presence of picrotoxin with a stimulus isolator (IsoFlex, AMPI) and a glass electrode placed dorsolateral to the recorded neuron, typically 100-200 μm away. Stimulus intensity was adjusted to yield EPSC amplitudes of ~400 pA. Stimulus duration was 300 μs. For evaluation of the paired-pulse ratio (PPR), two stimuli were given at variable interstimulus intervals (ISIs; 25, 50, 100, 200, 500 ms) with a 20 s intertrial interval. Three repetitions at each ISI were averaged to yield the PPR for that ISI. For monitoring of EPSC amplitude over time, two pulses delivered with 50 ms ISI were given every 20 s. Our high-frequency stimulation (HFS) protocol for induction of LTD consisted of 4 trials (1 s each, 10 s intertrial interval) of 100 Hz afferent stimulation (stimulation intensity calibrated to produce a 1.5 nA EPSC at −70 mV) paired with depolarization to −10 mV (Kreitzer and Malenka, 2007; Lerner and Kreitzer, 2012). Following the HFS protocol, the stimulation intensity was returned to the baseline level and EPSCs were monitored for a minimum of 30 additional minutes.

In slice experiments to validate use of the inhibitory DREADD hM4D (G_i), we prepared acute slices from animals coinjected with AAV5-DIO-ChR2-eYFP (UPenn Vector Core, 1 μl of 1:1 dilution) and AAV5-DIO-hM4D(G_i)-mCherry (UNC Vector Core, 1 μl). eYFP-positive striatal neurons were patched in the whole-cell current-clamp mode, with a potassium-based internal solution (see above). Optogenetic stimulation was delivered to the slice by a TTL-controlled LED (Olympus), passed through a ChR2 (473 nm) filter (Chroma) and the 40× immersion objective. LED intensity was adjusted to yield an output of ~1-2 mW at the slice. Light pulses were 5 ms in duration. To measure acute effects of CNO in slice physiology experiments, we targeted eYFP-negative neurons in the striatum or globus pallidus pars externa (GPe), in an area of mCherry fluorescence indicating local striatal axons were infected. These neurons were patched in whole-cell voltage-clamp mode, with a cesium chloride-based internal solution containing the following (in mM): 120 CsCl, 15 $CsMeSO_3$, 8 NaCl, 0.5 EGTA, 10 HEPES, 2 MgATP, 0.3 NaGTP, pH 7.3. IPSCs were elicited with optogenetic stimulation every 30 s.

Histology. Following behavioral, *in vivo* physiology, and chemogenetic experiments, mice were deeply anesthetized with IP ketamine-xylazine and transcardially perfused with 4% PFA in PBS. Before perfusion, electrode location was marked in implanted mice by electrolytic lesioning. After deep anesthesia, the implant was connected to a solid state, direct current Lesion Maker (Ugo Basile). A current of 100 μA was passed through each microwire for 5 s. After perfusion, the brain was dissected from the skull and postfixed overnight in 4% PFA, then placed in 30% sucrose at 4°C for 2-3 d for cryoprotection. The brain was then cut into 30 μm coronal sections on a freezing microtome (Leica), before washing in PBS and mounting in Vectashield Mounting Medium onto glass slides for subsequent imaging. All images were taken on a Nikon 6D conventional widefield microscope.

Experimental design and statistical analysis. The experimental design and statistical analysis of all key experiments are summarized in Table 1. This table includes planned sample sizes, statistical tests, *N* (animals), *n* (units or cells), *p* values, and the associated figures. Power calculations were performed based on either pilot data or the relevant literature. For behavioral experiments, we based power calculations on prior pharmacological studies in PNKD (Lee et al., 2012), as well as prior chemogenetic studies in dyskinesia (Alcacer et al., 2017), typically discounting the reported effect sizes by 50%. For slice electrophysiology experiments, we based power calculations on prior publications on striatal excitability (Planert et al., 2013; Fieblinger et al., 2014) and synaptic function (Kreitzer and Malenka, 2007), again typically discounting reported effect sizes by 50%. We aimed to achieve $>$90% power to detect a significant difference with a two-sided α of 0.05, using the statistical tests reported in the table.

Comparison groups are indicated in Results or the figures. In behavioral experiments, caffeine-induced dyskinesia scores were compared within-group at baseline (−30 to 0 min before caffeine) and 30-60 min after caffeine injection. In chemogenetic experiments, dyskinesia scores were compared at baseline (0-10 min) and at 40-60 min following CNO administration. Only one data point was collected per animal per behavioral state/manipulation.

For *in vivo* electrophysiological experiments, firing rate was compared before, during, and after dyskinetic periods, using the average firing rate from 0-30 min before injection, 30-60 min after injection, and 0-20 min after behavioral recovery (dyskinesia score of 2). In many cases, multiple neurons were recorded in each animal in each behavioral state, but each neuron was only sampled once per animal/manipulation.

In DREADD validation slice electrophysiological experiments, IPSC amplitude was compared before and 10-15 min after addition of CNO to the ACSF. Synaptic depression was analyzed by calculating the average EPSC amplitude during the 10 min baseline and 20-30 min following a manipulation (HFS or WIN55212 application). Changes in excitability

Table 1. Experimental design and analysis[a]

Key experiments	Figure	Comparison	Statistical Test	*N* (animals)	*n* (units/cells)	*p*	Planned sample size (from power calculation)
Intracranial caffeine infusion	1*D*	Between-group	MWU	5	NA	0.0128	$N = 6$ mice
Baseline firing rate of all MSNs	1*H*	Between-group	MWU	12 (WT), 16 (PNKD)	376 (WT), 350 (PNKD)	0.13	$N = 10$ mice, $n = 100$ units/group
Change in firing rate after caffeine	1*H*	Within-cell	WSR	12 (WT), 16 (PNKD)	230 (WT), 205 (PNKD)	0.0013 (WT), <0.0001 (PNKD)	$N = 10$ mice, $n = 100$ units/group
Baseline firing rate of dMSNs	1*I*	Between-group	MWU	5 (WT), 6 (PNKD)	66 (WT), 32 (PNKD)	0.33	$N = 5$ mice, $n = 40$ units/group
Change in dMSN firing rate after caffeine	1*I*	Within-cell	WSR	5 (WT), 6 (PNKD)	66 (WT), 32 (PNKD)	0.008 (WT), 0.32 (PNKD)	$N = 5$ mice, $n = 40$ units/group
Baseline firing rate of iMSNs	1*J*	Between-group	MWU	4 (WT), 7 (PNKD)	34 (WT), 68 (PNKD)	0.59	$N = 5$ mice, $n = 40$ units/group
Change in iMSN firing rate after caffeine	1*J*	Within-cell	WSR	4 (WT), 7 (PNKD)	21 (WT), 38 (PNKD)	0.59 (WT), <0.0001 (PNKD)	$N = 5$ mice, $n = 40$ units/group
Slice validation of Gi DREADD	1*C–E*	Within-cell	WSR	5	13	0.0016	$n = 7$ cells
Behavior with Gi DREADD	2*H, I*	Within-animal	WSR	9	NA	<0.0001	$N = 10$ mice/group
Behavior with Gs DREADD	3*B*	Between-group	MWU	9 (ctl), 10 (DREADD)	NA	0.00028	$N = 10$ mice/group
Change in dMSN excitability with caffeine	4*E–H*	Within-cell	WSR	5 (WT), 4 (PNKD)	7 (WT), 7 (PNKD)	0.31 (WT), 0.79 (PNKD)	$n = 7$ cells/group
Change in iMSN excitability with caffeine	5*E–H*	Within-cell	WSR	4 (WT), 4 (PNKD)	12 (WT), 7 (PNKD)	0.39 (WT), 0.039 (PNKD),	$n = 7$ cells/group
mEPSC frequency of dMSNs	6*B*	Between-group	ANOVA	13 (WT), 7 (PNKD), 9 (PNKD/dysk)	31 (WT), 21 (PNKD), 21 (PNKD/dysk)	0.42	$n = 20$ cells/group
mEPSC amplitude of dMSNs	6*C*	Between-group	ANOVA	13 (WT), 7 (PNKD), 9 (PNKD/dysk)	31 (WT), 21 (PNKD), 21 (PNKD/dysk)	0.45	$n = 20$ cells/group
Evoked EPSC, PPR in dMSNs	6*E*	Between-group	MWU	5 (WT), 6 (PNKD)	22 (WT), 24 (PNKD)	0.83	$n = 20$ cells/group
mEPSC frequency of iMSNs	7*B*	Between-group	ANOVA, HSD	15 (WT), 5 (PNKD), 7 (PNKD/dysk)	37 (WT), 21 (PNKD), 22 (PNKD/dysk)	0.0003	$n = 20$ cells/group
mEPSC amplitude of iMSNs	7*C*	Between-group	ANOVA, HSD	15 (WT), 5 (PNKD), 7 (PNKD/dysk)	37 (WT), 21 (PNKD), 22 (PNKD/dysk)	0.0018	$n = 20$ cells/group
mEPSC frequency caffeine	7*E*	Within-cell	WSR	4 (PNKD)	13 (PNKD)	0.01	$n = 10$ cells
Evoked EPSC, PPR in iMSNs	7*G*	Between-group	MWU	8 (WT), 11 (PNKD)	23 (WT), 23 (PNKD)	0.016	$n = 20$ cells/group
LTD of inputs onto iMSNs	7*H*	Within-cell	WSR	6 (WT), 7 (PNKD)	10 (WT), 8 (PNKD)	0.008 (WT), 0.15 (PNKD)	$n = 7$ cells/group
Evoked EPSC with WIN55212	7*I*	Between-group	MWU	5 (WT), 7 (PNKD)	7 (WT), 9 (PNKD)	<0.0001	$n = 7$ cells/group
Behavior with AM251	8*B*	Between-group	MWU	10 (PNKD)	NA	<0.0001	$N = 10$ mice/group
Change in firing rate after caffeine/AM251	8*D, E*	Within-cell	WSR	4 (PNKD)	18 (unID), 8 (iMSNs)	0.11 (unID), 0.643 (iMSNs)	$n = 10$ units/group
Behavior with JZL at 10 mg/kg caffeine	8*G*	Between-group	MWU	13 (PNKD)	NA	0.00008	$N = 10$ mice/group

[a]WSR, Wilcoxon Signed Rank Test; MWU, Wilcoxon Rank Sum or Mann–Whitney *U* test; HSD, Tukey's HSD.

or mEPSC frequency in response to acute caffeine application were analyzed by comparing a 10 min baseline period with the value 20-30 min after drug application.

Results

We investigated the physiological correlates of dyskinesia in the PNKD mouse model (Lee et al., 2012). In this model, animals show normal baseline movement, but ~5-10 min after IP injection of caffeine, PNKD mice develop markedly abnormal movement, including repetitive licking, gnawing, choreiform movements of the forepaws, and intermittent dystonic postures (Fig. 1*A*,*B*; Movie 1; $N = 24$ mice). WT littermates showed mild hyperactivity but no dyskinesias (Fig. 1*A*; $N = 15$ mice). To date, no definitive evidence indicates what site in the brain causes dyskinesia in PNKD. However, traditional models of basal ganglia function suggest that the striatum may be a key site. To determine whether local striatal caffeine infusion could trigger dyskinesia, we implanted infusion cannulae in the DLS (sensorimotor) of PNKD mice and WT littermates (Fig. 1*C*). Saline infusion did not trigger dyskinesias in WT or PNKD mice, but caffeine reliably triggered dyskinesia in PNKD mice (Fig. 1*D*; $p = 0.026$, $N = 5$ mice per group). The ability of local striatal caffeine to reproduce the behavioral effects of systemic caffeine administration suggests that abnormalities in striatum are critical for triggering dyskinetic attacks in PNKD.

We next explored the neurophysiological correlates of dyskinetic attacks within the striatum, taking advantage of the paroxysmal nature of this disorder. We implanted multielectrode arrays in the DLS (Fig. 1*E*,*F*). The single-unit activity of striatal MSNs was assessed before and after caffeine injection in PNKD mice and their WT littermates during open field behavior. In the nondyskinetic state (before injection), the firing rates of MSNs recorded in WT mice (1.33 ± 0.18 spikes/s; $n = 376$ units; $N = 12$ mice) did not differ from those recorded in PNKD animals (1.40 ± 0.10 spikes/s; $n = 350$ units; $N = 16$ mice; $p = 0.13$). Caffeine injection triggered mild hyperactivity and a modest increase in the average MSN firing rate in WT animals to 1.61 ± 0.09 spikes/s, with individual neurons showing both increases and decreases in firing rate (Fig. 1*H*; $n = 230$ units; $N = 12$ mice; $p = 0.0013$). Surprisingly, in PNKD animals, caffeine triggered a decrease in the average firing rate to 0.79 ± 0.18 spikes/s in parallel with dyskinesia (Fig. 1*H*; $n = 205$ units; $N = 16$ mice; $p < 0.0001$). Thus, in contrast to other models of dyskinesia and/or dystonia (Gernert et al., 1999; Liang et al., 2008), reduced striatal single-unit activity was observed during dyskinesia.

Based on classical models of basal ganglia function (DeLong, 1990), hyperkinetic movements are predicted to result from an increase in direct pathway activity, a decrease in indirect pathway activity, or both. Given the overall decrease in striatal firing we observed during dyskinesia, we hypothesized that iMSN firing might be suppressed after caffeine administration. To specifically record from striatal dMSNs or iMSNs, we used an optogenetic labeling approach (Kravitz et al., 2013; Jin et al., 2014), using Cre recombinase mouse lines that selectively label neurons composing the two pathways [Drd1-Cre (D1-cre) and Adora2a-Cre (A2a-Cre) for dMSNs and iMSNs, respectively (Gong et al., 2007; Gerfen et al., 2013)]. Mice were injected with an AAV encoding Cre-dependent channelrhodopsin-2 (ChR2) and implanted with optrode arrays. Positively identified single units showed short-latency firing to blue light pulses (Fig. 1*G*). We first examined whether baseline firing rates differed between identified dMSNs and iMSNs in WT and PNKD mice. The baseline firing rate of dMSNs did not differ between WT (1.72 ± 0.22 spikes/s; $n = 66$ dMSNs; $N = 5$ mice) and PNKD animals (1.66 ± 0.31 spikes/s; $n = 32$ dMSNs; $N = 6$ mice; $p = 0.33$), nor did the firing rates of iMSNs (1.42 ± 0.28 spikes/s in WT vs 1.40 ± 0.17 spikes/s in PNKD; $n = 34$, 68 iMSNs; $N = 4$, 7 mice, respectively; $p = 0.59$). As with the

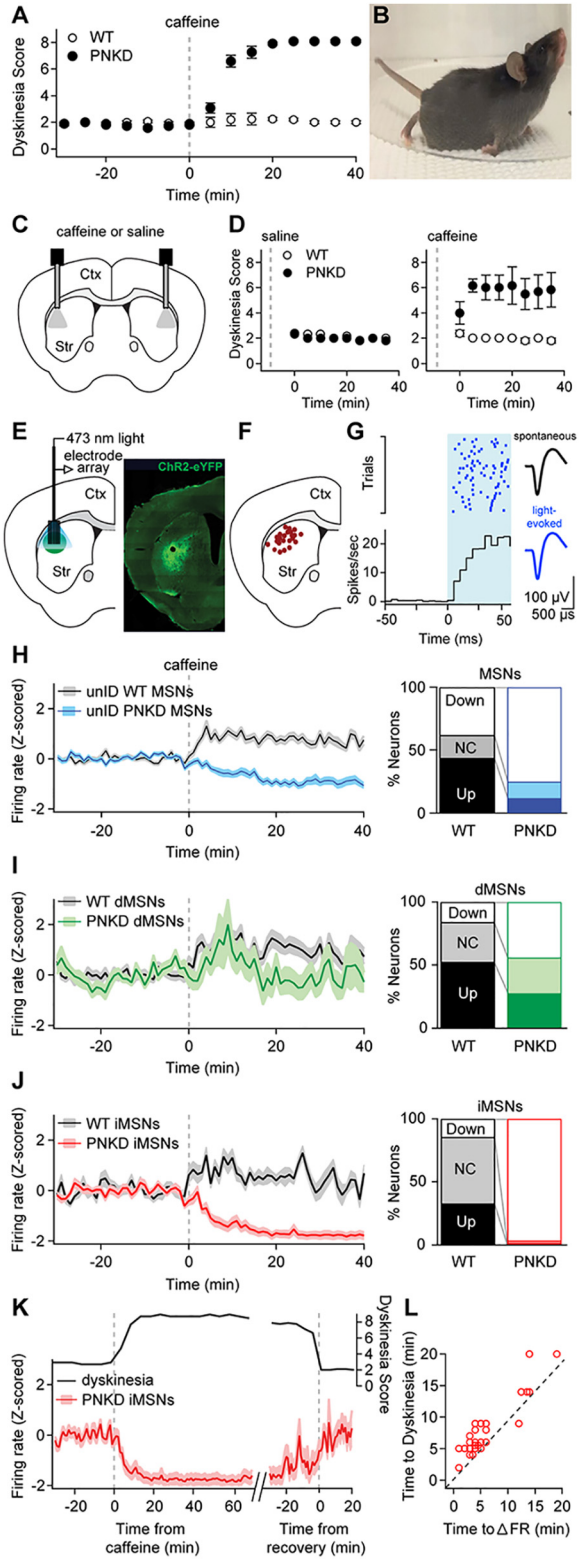

Figure 1. Striatal indirect pathway firing is profoundly decreased during dyskinesia in PNKD. ***A***, Dyskinesia scores of WT and PNKD mice treated with systemic caffeine (dotted line). ***B***, Dystonic posturing in a PNKD mouse. ***C***, Schematic diagram of bilateral infusion cannulae in the DLS. ***D***, Dyskinesias scores of WT and PNKD mice after bilateral intrastriatal infusion of saline (left) or caffeine (right). ***E***, Optrode recording configuration (left) and representative postmortem histology showing ChR2-eYFP and recording site in DLS. ***F***, Recording sites (confirmed by electrolytic lesioning). ***G***, Representative optogenetically identified unit, showing responses to blue light pulses (left) and average spontaneous and light-evoked waveforms (right). ***H–J***, Left, Average *Z*-scored firing rates of unidentified MSNs (***H***), optogenetically identified direct pathway MSNs (***I***), or indirect pathway MSNs (***J***) in WT and PNKD mice, before and after caffeine administration. Right, Percentage of units whose firing rates went up, down, or had no change (NC) after caffeine. ***K***, Dyskinesia score (black line) and *Z*-scored iMSN firing rates (red line) from PNKD animals monitored until recovery. ***L***, Plot of time to change in firing rate of iMSNs versus time to dyskinesia. Data are mean ± SEM.

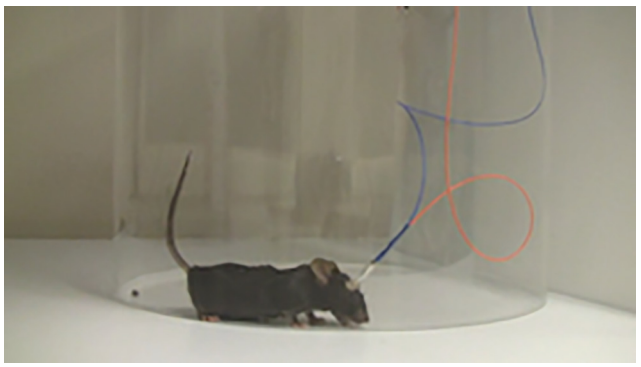

Movie 1. Caffeine induces abnormal movements in PNKD mice. A PNKD mouse was treated with caffeine (25 mg/kg, IP injection), which induced abnormal movements, including repetitive licking and forepaw movements. These movements occur intermittently for a period of hours after caffeine injection. [View online]

unidentified striatal recordings, these cell type-specific recordings suggest that there is no gross change in baseline striatal firing in PNKD mice versus healthy mice, consistent with normal motor behavior during this period.

We next tested whether the firing rate of optically identified dMSNs or iMSNs changed during caffeine-induced dyskinetic attacks. In dMSNs, caffeine injection evoked a variety of firing rate responses in both WT and PNKD animals (Fig. 1*I*). On average, dMSNs showed an increase in firing rate following caffeine injection in WT animals ($n = 66$ dMSNs; $N = 5$ mice; $p = 0.008$), but not in PNKD animals ($n = 32$ dMSNs, $N = 6$ mice; $p = 0.32$). However, we found significant changes in iMSN activity that developed in parallel with dyskinesia in PNKD mice. In WT iMSNs, a variety of individual responses were seen, but average firing rate was unchanged after caffeine injection (Fig. 1*J*; $n = 21$ iMSNs, $N = 4$ mice; $p = 0.59$). In contrast, the firing rate of PNKD iMSNs dramatically decreased, on average to 0.09 ± 0.03 spikes/s (Fig. 1*J*; $n = 38$ iMSNs, $N = 7$ mice; $p < 0.0001$). To investigate how the caffeine-triggered decrease in iMSN activity might be related to dyskinesia in PNKD mice, we looked more closely at the timing of firing rate and behavioral changes. In extended recording sessions lasting 4-6 h, the timing of iMSN firing rate changes closely paralleled both the onset and offset of dyskinesia, with decreased firing rate during dyskinesias and restoration of baseline firing rate at the time of behavioral recovery (Fig. 1*K*). Furthermore, in all but one PNKD iMSN recorded, the firing rate decreased significantly before the onset of dyskinesia (Fig. 1*L*). These findings indicate that, in PNKD mice, caffeine-induced dyskinesia is tightly correlated with suppression of iMSN firing.

Reduced iMSN firing rates and dyskinesia are strongly correlated in PNKD, but these findings do not demonstrate causality. Indeed, dyskinesia may be characterized by changes in activity in many brain regions, some causative and others the result of the altered experience of a dyskinetic animal. To determine whether inhibition of iMSN activity is sufficient to cause dyskinesia in the absence of caffeine, we used a chemogenetic approach. We

expressed the inhibitory DREADD, hM4D(G_i-coupled) or a control fluorophore (mCherry) in iMSNs of the DLS of both WT; A2a-Cre and PNKD;A2a-Cre mice (Fig. 2*A*). To validate the use of hM4D, we first performed whole-cell *ex vivo* recordings in brain slices from a subset of mice coinjected with Cre-dependent ChR2-eYFP (Fig. 2*A–E*). Brief blue light pulses evoked spiking in ChR2-eYFP-positive iMSNs (Fig. 2*B*). Voltage-clamp recordings in postsynaptic eYFP-negative MSNs (Fig. 2*C*) or GPe neurons (Fig. 2*D*) showed light-evoked IPSCs. As expected (Bock et al., 2013; Stachniak et al., 2014), application of the DREADD agonist CNO reduced the amplitude of IPSCs onto both MSNs and GPe neurons (Fig. 2*C–E*; $n = 13$ striatal, $n = 5$ GPe cells, $N = 5$ mice, $p = 0.0016$). We repeated these experiments in slices from PNKD;A2a-Cre mice and found that CNO also reduced light-evoked IPSC amplitude in the striatum and GPe (Fig. 2*E*; $n = 7$ striatal, $n = 5$ GPe cells, $N = 3$ mice, $p = 0.03$), confirming that the G_i-coupled DREADD worked at least as well in PNKD animals. Using whole-cell current-clamp recordings, we also observed a modest hyperpolarization of resting membrane potential in mCherry-positive iMSNs after CNO application (Fig. 2*E*; 2.7 ± 1.1 mV; $n = 7$ iMSNs, $N = 2$ mice), as has been seen in other studies using the G_i-coupled DREADD in the striatum (Kozorovitskiy et al., 2012). These findings validate the use of G_i-coupled DREADDs in the striatum.

To determine whether activating G_i-DREADDs in striatal iMSNs could cause dyskinesia, we tested the effects of CNO on animals in the open field. After habituation to daily IP saline injections, we scored motor behavior after injection of saline or CNO (Fig. 2*F,G*). Administration of saline did not evoke dyskinesia in any group (Fig. 2*H,I*, left panels; $N = 6$-10 mice per group). CNO administration did not result in abnormal movements in mCherry-injected WT;A2a-Cre or PNKD;A2a-Cre mice (Fig. 2*H,I*, right panels; $N = 6$-8 mice per group, $p = 0.373$, 0.17, respectively) nor in G_i-coupled DREADD-injected WT mice (Fig. 2*H*, right; $N = 8$ mice, $p = 0.9$), but in PNKD;A2a-Cre mice, CNO triggered dyskinesia (Fig. 2*I*, right; $N = 9$ mice, $p < 0.0001$). These results demonstrate that chemogenetic inhibition of iMSNs is sufficient to cause dyskinesia in PNKD mice, but not WT mice.

We next tested whether chemogenetic activation of iMSNs might blunt dyskinesia. We expressed the activating DREADD hM3D(G_s-coupled) in PNKD;A2a-Cre mice (Fig. 3*A*). After habituation to IP injections, saline or CNO was administered 20 min before injection with caffeine (Fig. 3*B*, top). If reductions in iMSN output are required for dyskinesia in PNKD mice, then pretreatment with CNO should reduce the severity of caffeine-induced dyskinetic attacks. While pretreatment with saline did not prevent caffeine-induced attacks (Fig. 3*B*, middle), pretreatment with CNO reduced dyskinesia in G_s-coupled DREADD-expressing mice compared with mCherry-expressing controls ($N = 9$ or 10 mice per group; $p = 0.00028$; Fig. 3*B*, bottom), suggesting that reductions in iMSN activity are necessary for dyskinesia in PNKD.

To further investigate the mechanism underlying onset of dyskinesia, we reasoned that caffeine, an antagonist at G_s-coupled adenosine A2a receptors, might trigger dyskinetic attacks in PNKD through regulation of either the intrinsic excitability of iMSNs or the strength of their excitatory inputs. Within the basal ganglia and its connections, A2a receptors are selectively expressed on striatal iMSNs (Schiffmann et al., 1991), which might account for the cell type selectivity of the inhibition we observed during dyskinesia. In order to test whether the intrinsic excitability of dMSNs or iMSNs was altered in PNKD

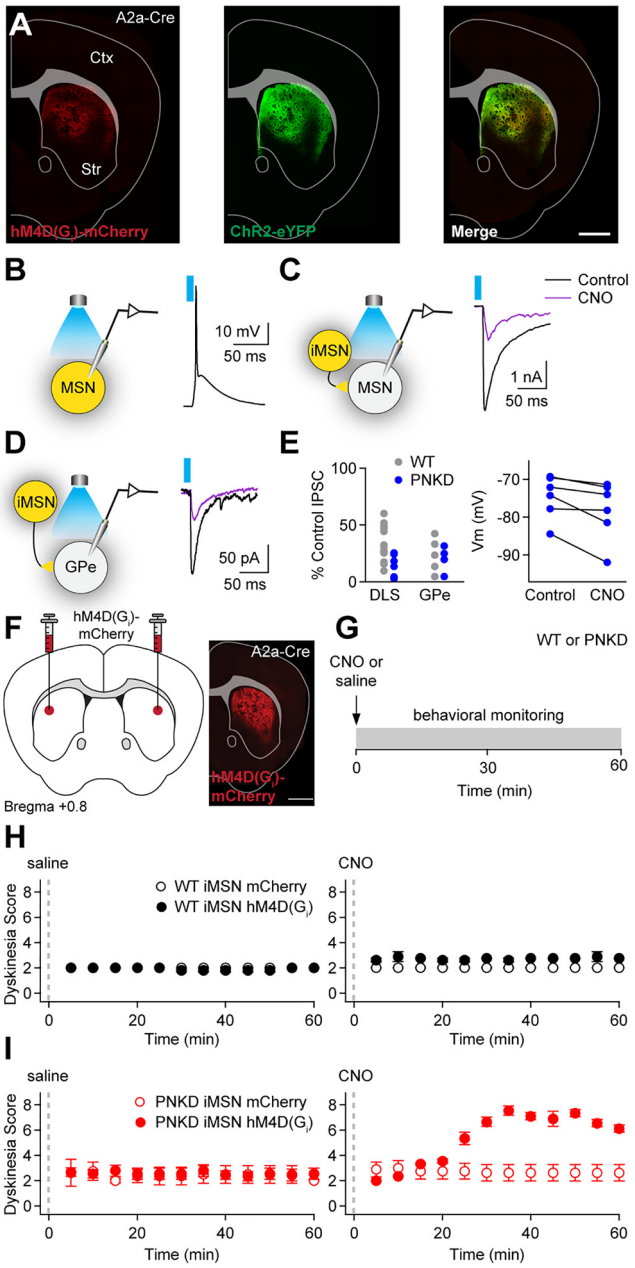

Figure 2. Chemogenetic inhibition of striatal iMSNs triggers dyskinetic attacks in PNKD mice. A2a-Cre mice were injected in the DLS with AAV5-DIO-hM4D(G_i)-mCherry or AAV5-DIO-mCherry. ***A–E***, Mice were also injected with AAV5-DIO-ChR2-eYFP. ***A***, Representative coronal sections showing expression of hM4D(G_i)-mCherry (left), ChR2-eYFP (middle), and merged (right) in the DLS. ***B–E***, Whole-cell recordings of MSNs (***B***,***C***) and GPe (***D***) neurons. Recording configurations are schematized at left in each panel. ***B***, Representative current-clamp recording from an eYFP-positive striatal neuron (putative iMSN), showing a light-evoked action potential in response to a 5 ms pulse of blue light. ***C***, ***D***, Representative voltage-clamp recordings from an eYFP-negative MSN (***C***) or GPe neuron (***D***), showing light-evoked IPSCs before (black) and after (purple) application of CNO. ***E***, Left, Summary of IPSC amplitude in the DLS and GPe after CNO application. Right, Resting V_m of iMSNs before and after CNO application. ***F***, Schematic diagram showing bilateral injection of virus encoding hM4D-mCherry or mCherry, and postmortem tissue showing expression. ***G***, Behavioral session timeline. ***H***, ***I***, Dyskinesia scores of WT mice treated with saline (***H***, left) or CNO (***H***, right), PNKD mice treated with saline (***I***, left), or CNO (***I***, right). Data are mean ± SEM. Scale bar, 1 mm.

mice, we performed whole-cell *ex vivo* recordings in slices of PNKD or WT mice, using fluorophore lines in which dMSNs and iMSNs can be visually identified (Figs. 4*A,B*, 5*A,B*) (Doyle et al., 2008; Shuen et al., 2008). In order to reduce the likelihood of

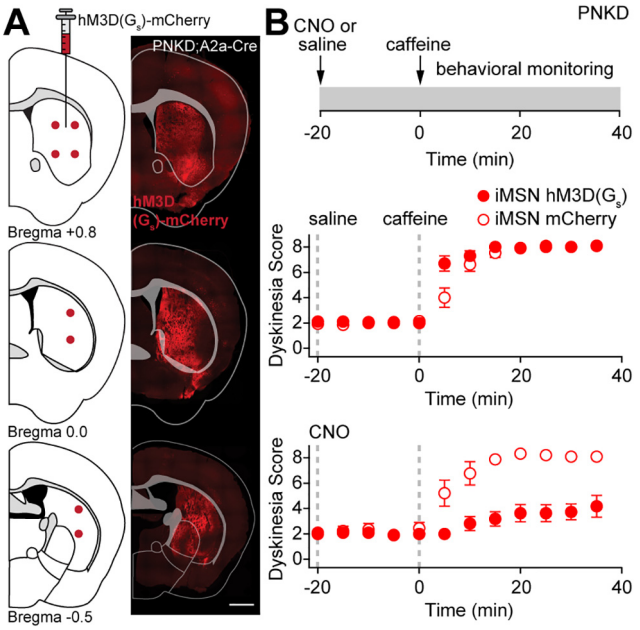

Figure 3. Chemogenetic activation of striatal iMSNs blunts dyskinetic attacks in PNKD mice. The striatum of PNKD;A2a-Cre mice was injected with AAV5-DIO-hM3D(G_s)-mCherry or AAV5-DIO-mCherry. ***A***, Postmortem striatal mCherry expression. ***B***, Top, Behavioral session timeline. Middle, Bottom, Dyskinesia score in animals pretreated with saline (middle) or CNO (bottom) before caffeine. Data are mean ± SEM. Scale bars, 1 mm.

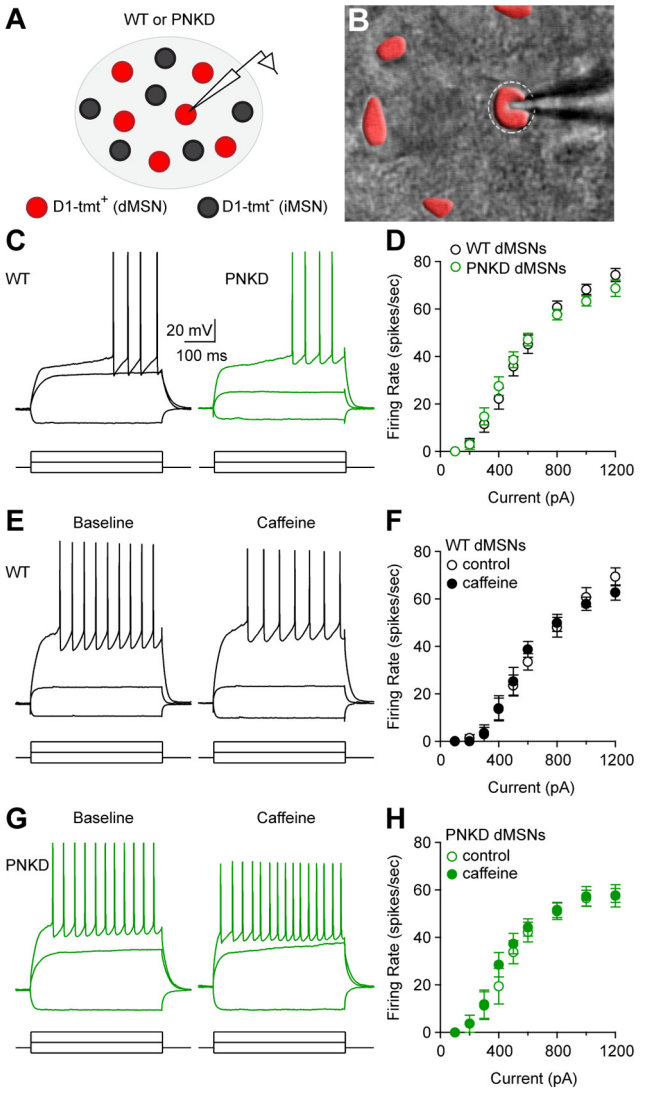

Figure 4. Intrinsic excitability is not significantly altered in WT or PNKD dMSNs. Current-clamp recordings from dMSNs in WT and PNKD slices. ***A***, ***B***, Schematic diagram showing identification of tdTomato-positive dMSNs and recording configuration. ***C***, Representative WT (black) and PNKD (green) dMSN responses to current injections (−100, 100, and 300 pA steps). ***D***, Summary of input-output curves in WT and PNKD dMSNs. ***E***, Representative WT dMSN responses before and after caffeine application. ***F***, Summary of input-output curves in WT dMSNs before and after caffeine. ***G***, Representative PNKD dMSN responses to before and after caffeine application. ***H***, Summary of input-output curves in PNKD dMSNs before and after caffeine. Data are mean ± SEM.

stress-induced dyskinetic attacks around the time of death, we habituated animals to daily saline injections before preparation of brain slices. As these brain slices should represent the nondyskinetic state in PNKD mice, we hypothesized that basic electrophysiological properties would not differ between neurons in PNKD and WT mice. We found that input resistance, resting membrane potential, and rheobase were similar in dMSNs from WT ($n = 24$ cells, $N = 7$ mice) and PNKD slices ($n = 20$ cells, $N = 4$ mice, $p = 0.25$; Table 2). To measure excitability, we injected current steps of varying amplitude, and measured the output firing rate (Fig. 4*C*). The relationship between input current and output firing rate was very similar in WT and PNKD dMSNs (Fig. 4*D*). The similar *ex vivo* intrinsic properties of WT and PNKD dMSNs were consistent with the comparable baseline firing rates we observed in dMSNs in freely moving mice.

We next examined whether acute caffeine application could evoke changes in the excitability of dMSNs in WT or PNKD slices. As dMSNs do not express A2a receptors (Schiffmann et al., 1991), we reasoned caffeine would not trigger significant changes in excitability. Indeed, acute caffeine application did not alter dMSN firing response gain in WT (Fig. 4*E*,*F*; $n = 7$, $N = 5$, $p > 0.05$) or PNKD slices (Fig. 4*G*,*H*; $n = 7$, $N = 4$, $p > 0.05$). These results are consistent with the hypothesis that intrinsic properties of dMSNs are not strongly modulated by caffeine.

We next tested the intrinsic excitability of iMSNs from WT and PNKD mice, using the same methods. Resting membrane potential and input resistance did not differ between iMSNs recorded in WT ($n = 22$, $N = 8$) and PNKD mice ($n = 22$, $N = 4$; Table 2). We were able to confirm the previously reported finding (Kreitzer and Malenka, 2007; Day et al., 2008; Planert et al., 2013) that iMSNs are more excitable than dMSNs (Figs. 4*D*, 5*D*; $p = 0.04$), but we did not observe differences in the rheobase or firing response gain between WT and PNKD iMSNs (Fig. 5*C*,*D*; Table 2). If the dyskinesia-associated reductions in the firing rate of PNKD iMSNs *in vivo* were mediated by reductions in intrinsic excitability, we would expect to see a decrease in intrinsic excitability in response to caffeine application. However, caffeine did not trigger notable differences in the evoked firing of iMSNs in WT (Fig. 5*E*,*F*, $n = 12$, $N = 4$, $p = 0.39$) or PNKD slices (Fig. 5*G*,*H*, $n = 7$, $N = 4$, $p > 0.05$). The negligible effects of caffeine on intrinsic excitability of iMSNs are consistent with previously published evidence suggesting that A2a receptors primarily modulate excitatory synaptic inputs onto iMSNs (Higley and Sabatini, 2010).

A2a receptors expressed in iMSNs are known to regulate endocannabinoid release, which is implicated in synaptic depression on both short and long timescales (Gerdeman et al., 2002; Narushima et al., 2006; W. Shen et al., 2008; Lerner and Kreitzer, 2012). Endocannabinoid-dependent LTD is presynaptically expressed and characterized by a reduction in the probability of transmitter release and decreased mEPSC frequency, but not amplitude (Choi and Lovinger, 1997a,b). To

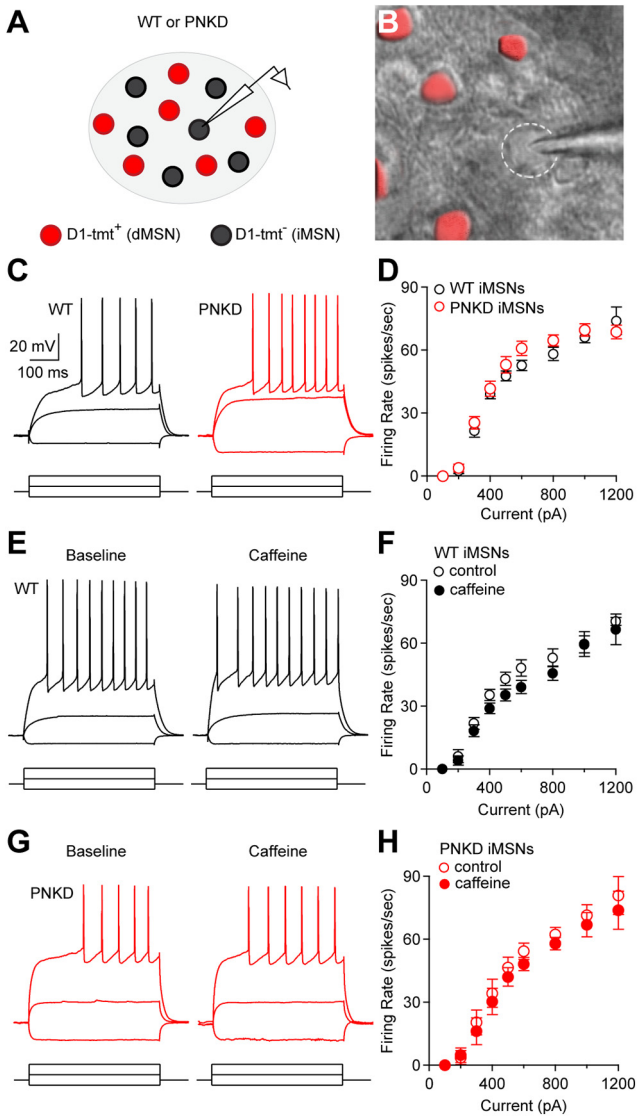

Figure 5. Intrinsic excitability is not significantly altered in WT or PNKD iMSNs. Current-clamp recordings from iMSNs in WT and PNKD slices. ***A***, ***B***, Schematic diagram showing identification of tdTomato-negative iMSNs and recording configuration. ***C***, Representative WT (black) and PNKD (green) iMSN responses to current injections (−100, 100, and 300 pA steps). ***D***, Summary of input-output curves in WT and PNKD iMSNs. ***E***, Representative WT iMSN responses before and after caffeine application. ***F***, Summary of input-output curves in WT iMSNs before and after caffeine. ***G***, Representative PNKD iMSN responses to before and after caffeine application. ***H***, Summary of input-output curves in PNKD iMSNs before and after caffeine. Data are mean ± SEM.

test whether excitatory synaptic transmission is altered onto dMSNs or iMSNs in PNKD mice, we performed whole-cell voltage-clamp recordings. We compared slices from mice representing three conditions: WT mice, PNKD mice in the nondyskinetic state, and PNKD mice in the dyskinetic state (stress-induced). We first measured mEPSCs in dMSNs (Fig. 6*A–C*). We saw no significant differences in mEPSC amplitude ($p = 0.45$) or frequency ($p = 0.42$) between the three groups ($n = 21$-31 neurons and $N = 6$-13 mice per group). Furthermore, we did not observe acute changes in dMSN mEPSC amplitude or frequency after application of caffeine in PNKD slices (data not shown; $n = 9$, $N = 4$, $p > 0.05$). We observed similar evoked EPSCs in dMSNS from WT and PNKD slices, as measured by pulse ratio (PPR; Fig. 6*D*,*E*; $n = 22$, 24 cells, $N = 5$, 6 mice respectively; $p = 0.83$). These findings in *ex vivo* recordings indicate PNKD is not associated with marked changes in dMSN excitability or synaptic function.

Based on our *in vivo* recordings, we predicted marked changes in iMSN synaptic function in *ex vivo* slices from PNKD mice in the dyskinetic state. We first measured mEPSCs in iMSNs from WT mice, nondyskinetic PNKD mice, and dyskinetic PNKD mice (Fig. 7*A–C*). Although mEPSC amplitude was similar across the groups, we observed small (9%-12%), but significant, differences between iMSNs from WT mice ($n = 37$, $N = 15$), nondyskinetic PNKD mice ($n = 21$, $N = 5$), and dyskinetic PNKD mice ($n = 22$, $N = 7$, $p = 0.0018$). However, iMSN mEPSC frequency was more substantially (25%-38%) reduced in slices from dyskinetic PNKD mice compared with WT littermates or nondyskinetic PNKD mice ($p = 0.0003$). We could elicit similar acute reductions in mEPSC frequency by applying caffeine on slices from nondyskinetic PNKD mice (Fig. 7*A*,*D*,*E*; $n = 13$, $N = 4$, $p = 0.0001$). Together, these results support the idea that there may be a reduction in the number of excitatory synapses and/or probability of release onto iMSNs in dyskinetic PNKD animals, consistent with prior observations of altered exocytosis in PNKD (Y. Shen et al., 2015). Also consistent with a reduction in the probability of release, at 40 Hz stimulation, we found increased PPR of evoked EPSCs in iMSNs from dyskinetic PNKD animals (Fig. 7*F*,*G*; $n = 23$ cells per group; $N = 8$,11 mice; $p = 0.016$). If these reductions in excitatory synaptic input onto iMSNs were the result of *in vivo* LTD, we predicted that LTD might be occluded in *ex vivo* slices from dyskinetic animals. To test this hypothesis, we recorded evoked EPSCs before and after a standard high-frequency (HFS) LTD protocol (Kreitzer and Malenka, 2007; Lerner and Kreitzer, 2012). In iMSNs from WT slices, LTD was robust (Fig. 7*H*; $n = 10$ cells; $N = 6$ mice; $p = 0.008$), but in iMSNs from PNKD animals, LTD was absent ($n = 8$ cells; $N = 7$ mice; $p = 0.15$), suggesting that it might be occluded. One of the major cellular mechanisms in presynaptic striatal LTD is release of endocannabinoids and CB1 receptor-dependent changes in presynaptic probability of release (Gerdeman et al., 2002; Kreitzer and Malenka, 2007). If this machinery had already been engaged in PNKD mice *in vivo*, then further endocannabinoid-mediated reductions in synaptic responses would be smaller than otherwise predicted. Indeed, the endocannabinoid agonist WIN55212 produced less synaptic depression in PNKD compared with WT iMSNs (Fig. 7*I*; $n = 7$, 9 cells; $N = 5$, 7 mice; $p < 0.0001$). These findings show a pathway-specific disruption in excitatory neurotransmission onto iMSNs in symptomatic PNKD animals, which may represent a cellular and synaptic substrate of dyskinesia in this model.

If depression of iMSN synaptic inputs leads to reduced iMSN activity, in turn causing dyskinesia, then preventing presynaptic CB1 activation should reduce or prevent dyskinetic attacks in PNKD mice. To test this hypothesis, we administered the CB1 antagonist AM251 to PNKD mice, before caffeine treatment (Fig. 8*A*). In vehicle-pretreated animals, caffeine triggers dyskinetic attacks, as expected (Fig. 8*B*, $N = 10$ mice, $p < 0.0001$), However, in AM251-pretreated mice, attack severity was strongly reduced ($N = 10$ mice, $p < 0.0001$), suggesting that endocannabinoid signaling is necessary for caffeine-induced dyskinesia. To explore whether AM251 might prevent dyskinetic attacks by blunting or preventing a loss of iMSN activity, we performed additional striatal single-unit recordings in PNKD animals during behavioral sessions (Fig. 8*C*,*D*). Administration of AM251 itself caused a modest reduction in MSN firing rates, from 1.31 ± 0.38 to 1.03 ± 0.38 spikes/s ($n = 18$ units, $N = 4$

Table 2. Intrinsic properties of WT and PNKD dMSNs and iMSNs[a]

Excitability parameters	WT dMSNs ($n = 24/N = 7$)	PNKD dMSNs ($n = 20/N = 4$)	p	WT iMSNs ($n = 22/N = 8$)	PNKD iMSNs ($n = 22/N = 4$)	p
R_{in} (MOhms)	104 ± 10	118 ± 18	0.25	160 ± 15	136 ± 10	0.25
V_m (mV)	(−85) ± 1.6	(−86.1) ± 1.3	0.95	(−89.2) ± 1.9	(−89.4) ± 1.6	0.66
Rheobase (pA)	400 ± 30	355 ± 22	0.26	283 ± 17	287 ± 21	0.87
Firing response gain (spikes/s/nA)	53 ± 4	49 ± 4	0.25	56 ± 3	60 ± 4	0.16

[a]*N*, *n* refer to the number of animals and cells, respectively.

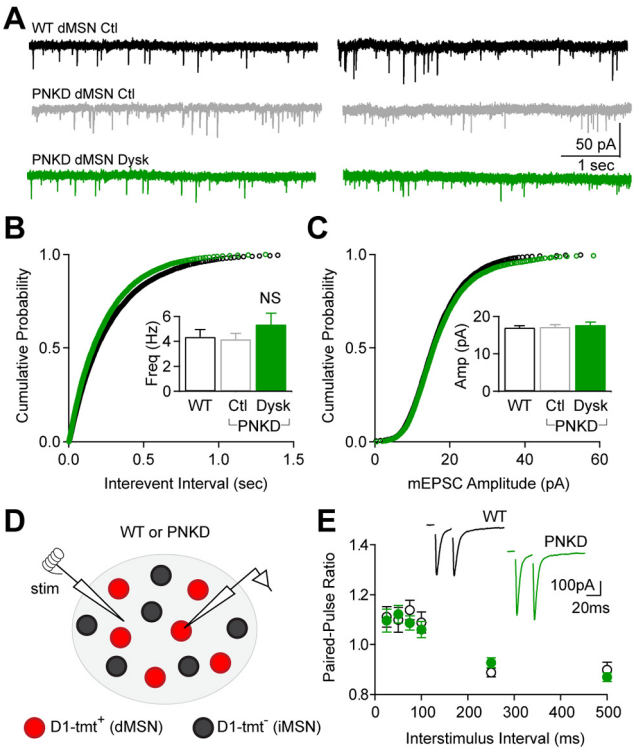

Figure 6. Synaptic properties are unaltered in dMSNs in PNKD. Voltage-clamp recordings from dMSNs in WT and PNKD slices ***A***, Representative traces of mEPSCs from WT (black), nondyskinetic PNKD (gray), and dyskinetic PNKD (green) dMSNs. ***B***, mEPSC frequency cumulative histogram from WT and PNKD dMSNs. Inset, Average mEPSC frequencies from WT (black open), nondyskinetic (gray open), and dyskinetic (green closed) PNKD mice. ***C***, mEPSC amplitude cumulative histogram. Inset, Average mEPSC amplitudes from WT (black open), nondyskinetic (gray open), and dyskinetic (green closed) PNKD mice. ***D***, Schematic diagram showing recording configuration, including local intrastriatal electrical stimulation. ***E***, Average PPR of evoked EPSCs in dMSNs from WT and PNKD mice. Inset, Representative EPSCs with 25 ms ISI. Data are mean ± SEM.

mice, $p = 0.02$). In contrast to control experiments, in which caffeine induced robust dyskinetic attacks and decreases in both unidentified (Fig. 1*H*) and iMSN firing rates (Fig. 1*J*), caffeine did not cause a significant change in unidentified MSN or iMSN firing rates after AM251 pretreatment (Fig. 8*D*,*E*; $n = 18$, 8 units; $N = 4$ mice; $p = 0.11$ and 0.643, respectively). These findings identify a candidate mechanism underlying iMSN suppression in PNKD, and further bolster our main hypothesis that reductions in indirect pathway activity are critical for the expression of dyskinesia in this model.

If endocannabinoid signaling is required for dyskinesia induction, we theorized that potentiating endocannabinoid signaling might lower the threshold for dyskinesia in PNKD mice. Previous work suggested that, *in vivo*, A2a antagonists increase the endocannabinoid 2-arachidonoylglycerol (Lerner et al., 2010), which is metabolized by monoacylglycerol lipase (MAGL). To test whether potentiating endocannabinoid signaling could lower the threshold for caffeine-induced dyskinesia in PNKD mice, we administered the MAGL inhibitor JZL184 (16 mg/kg) or vehicle (Long et al., 2009) in conjunction with lower doses of caffeine (2 and 10 mg/kg) that are less likely to cause dyskinesia (Fig. 8*F*,*G*) than the moderate doses (25 mg/kg) used elsewhere in our study. At the lowest dose (2 mg/kg) of caffeine, neither vehicle- nor JZL184-pretreated animals developed dyskinesias (Fig. 8*F*). At 10 mg/kg of caffeine, vehicle-treated animals developed modest behavioral abnormalities, including hyperactivity and exploratory behavior. However, the combination of JZL184 pretreatment and 10 mg/kg caffeine yielded greater dyskinesia than in vehicle-pretreated animals (Fig. 8*G*). These results suggest that enhancing or prolonging endocannabinoid signaling can lower the threshold for induction of dyskinesia in PNKD mice.

Discussion

This study tested the hypothesis that, in the PNKD mouse model, striatal circuit dysfunction contributes to dyskinetic attacks. We found that caffeine-induced dyskinetic attacks were paralleled by a profound reduction in the firing rate of striatal iMSNs. Reduced indirect pathway output appears to be necessary and sufficient for the generation of dyskinesia in the PNKD model, as chemogenetic manipulations of iMSNs yielded bidirectional regulation of dyskinesia. Further, using *ex vivo* slice recordings, a potential cellular mechanism for suppression of iMSN activity was identified: endocannabinoid-mediated synaptic depression of excitatory synapses onto iMSNs, which is known to be regulated by cAMP levels and A2A receptors (W. Shen et al., 2008; Lerner and Kreitzer, 2012). Indeed, pharmacological blockade of CB1 receptors *in vivo* blunted or prevented caffeine-induced dyskinetic attacks in PNKD mice. The predominant role of reduced indirect pathway activity in PNKD contrasts to dyskinesias seen in other disorders.

In some ways, the key role of iMSNs in the PNKD mouse model is not surprising. In the classic hyperkinetic movement disorder, Huntington's disease, postmortem studies suggest that early neurodegeneration may target iMSNs over dMSNs (Reiner et al., 1988). In LID, there are coincident increases in dMSN activity and decreases in iMSN activity (Parker et al., 2018; Ryan et al., 2018). Although aberrant direct pathway activity appears to be a major driver of dyskinetic movements in this disorder (Perez et al., 2017; Ryan et al., 2018), recent work has implicated iMSN activity as a contributor (Alcacer et al., 2017). One reason that iMSN activity may be critical for normal movements is that, by virtue of their extensive inhibitory collaterals within the striatum (Smith et al., 1998; Taverna et al., 2008; Dobbs et al., 2016; Wei et al., 2017), and through their downstream regulation of brainstem and thalamocortical motor circuits (Oldenburg and Sabatini, 2015; Roseberry et al., 2016), they are key to the normal ability to suppress competing motor programs (Cui et al., 2013; Tecuapetla et al., 2014, 2016). Broad loss of the inhibitory influence of iMSNs, either through neurodegeneration (as in Huntington's disease) or through reductions in firing rate or synchronization (as in PNKD and other "functional" forms of

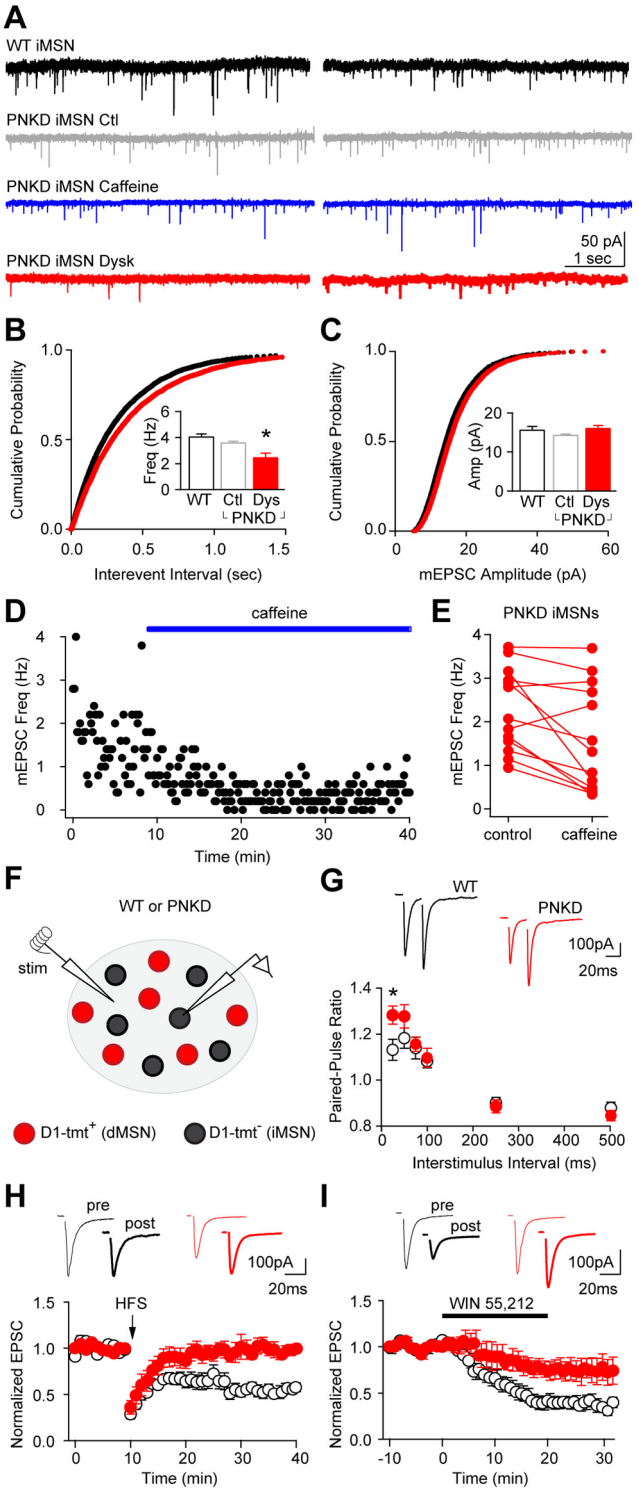

Figure 7. Excitatory transmission is reduced onto iMSNs in dyskinetic PNKD mice. Voltage-clamp recordings from iMSNs in WT and PNKD slices. ***A***, Representative mEPSC traces from WT (black), nondyskinetic PNKD before and after caffeine (gray and blue), and dyskinetic PNKD (red) iMSNs. ***B***, mEPSC frequency cumulative histogram (inset: averages) from WT, nondyskinetic (gray), and dyskinetic PNKD (red) iMSNs. ***C***, mEPSC amplitude cumulative histogram (inset: averages). ***D***, mEPSC frequency in a representative PNKD iMSN in response to acute application of caffeine. ***E***, Summary of mEPSC frequency before and after caffeine application. Each pair of dots represents one iMSN. ***F***, Schematic diagram showing recording configuration, including local intrastriatal electrical stimulation. ***G***, Average PPR of evoked EPSCs from WT and PNKD mice. Inset, Representative evoked EPSCs with 25 ms ISI. ***H***, Top, Representative evoked EPSCs before (thin line) and after (thick line) HFS. Bottom, Normalized EPSC amplitude in WT before and after HFS. ***I***, Top, Representative evoked EPSCs before and after application of WIN55212. Bottom, Normalized evoked EPSC amplitude in WT and PNKD iMSNs treated with WIN55212. Data are mean ± SEM.

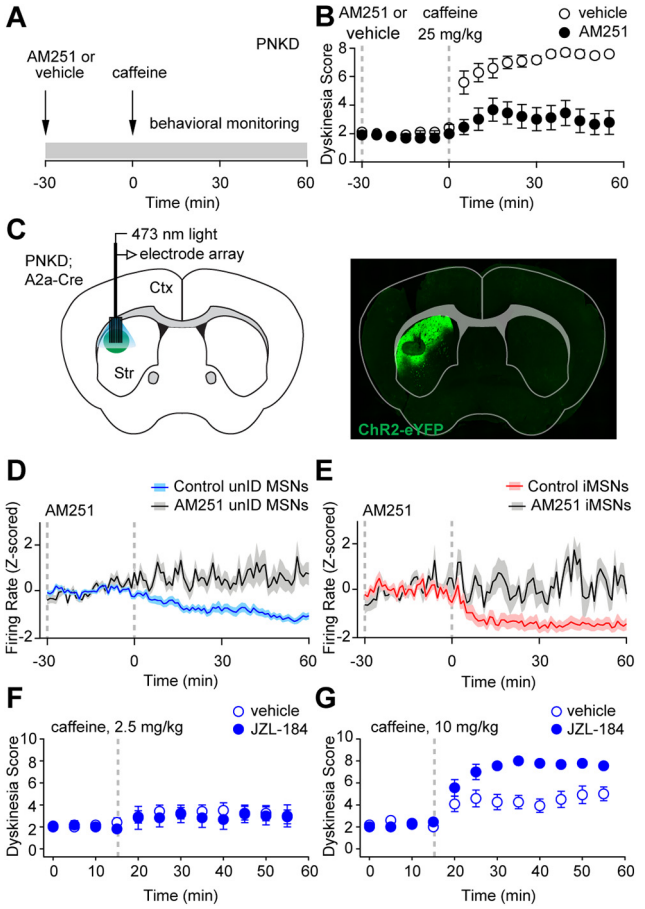

Figure 8. Endocannabinoid signaling bidirectionally regulates dyskinetic attacks in PNKD mice. ***A–E***, PNKD mice were pretreated with the endocannabinoid antagonist AM251 or vehicle before caffeine injection (25 mg/kg). ***A***, Experimental timeline. ***B***, Dyskinesia score in PNKD mice during these trials. ***C***, Left, Schematic of recording configuration. Right, Postmortem histology showing expression of ChR2-eYFP. ***D***, ***E***, Average *Z*-scored firing rates of all MSNs (***D***) and optically identified iMSNs (***E***) from PNKD mice treated with caffeine, with or without AM251 pretreatment. ***F***, ***G***, Dyskinesia scores in PNKD mice pretreated with the MAGL inhibitor JZL184 or vehicle before caffeine injection at 2 mg/kg (***F***) or 10 mg/kg (***G***). Data are mean ± SEM.

dyskinesia), could lead to increased activity in neighboring dMSN ensembles, decreasing the threshold for triggering movements facilitated by these ensembles (Burke et al., 2017). Although not linked to dyskinesia per se, a larger ensemble of activated dMSNs has been observed in parkinsonian mice treated with levodopa (Maltese et al., 2021). This type of microcircuit phenomenon might explain why voluntary movement can exacerbate chorea or dystonia in the same body segment (Berardelli et al., 1998; Albanese et al., 2013). Dyskinesias may thus represent an "overflow" of normal motor commands (Mink, 1996).

Interestingly, we found that chemogenetic suppression of iMSNs triggered dyskinesia in PNKD mice, but not in their WT littermates. This observation suggests that iMSN suppression (to the extent possible with DREADDs) alone is not sufficient to cause involuntary movement in otherwise normal basal ganglia

circuitry, consistent with another group's findings in a mouse model of Parkinson's disease (Alcacer et al., 2017). Additional cellular or circuit changes in PNKD, such as altered synaptic connectivity or aberrant biochemical signaling, may amplify the effects of chemogenetic inhibition, leading to increased vulnerability to dyskinesia. Precedent for downstream amplification of striatal signaling has been observed in a mouse model of Parkinson's disease/LID at striatonigral synapses (Borgkvist et al., 2015). In PNKD, a similar phenomenon might occur at intrastriatal and/or striatopallidal synapses, amplifying the effect of reduced iMSN activity. Several studies suggest that dopamine reduces the efficacy of both intrastriatal (Tecuapetla et al., 2009; Dobbs et al., 2016) and striatopallidal (Dayne Mayfield et al., 1996; Wei et al., 2013; Jijón-Lorenzo et al., 2018) synapses. Indeed, in parkinsonian mice, these synapses may become particularly sensitive to dopamine (Wei et al., 2013). If dopamine release is dysregulated in PNKD (Lee et al., 2012), it could further reduce synaptic efficacy of the indirect pathway.

We found that excitatory inputs, but not intrinsic excitability, were altered in iMSNs in brain slices from dyskinetic PNKD animals. Interestingly, excitatory inputs onto iMSNs from carefully habituated, nondyskinetic PNKD mice were similar to those onto WT iMSNs, and acute application of caffeine induced a reduction in mEPSC frequency. dMSNs, in contrast, showed little to no differences between WT and PNKD mice. These observations are consistent with the idea that aberrant synaptic plasticity may contribute to movement disorders (Deffains and Bergman, 2015). Alterations in striatal LTD have been observed in other animal models of hyperkinetic disorders, such as primary dystonias, drug-induced dyskinesias, and Huntington's disease (Picconi et al., 2003, 2006; Martella et al., 2009; Avchalumov et al., 2013; Sepers et al., 2018; Ghiglieri et al., 2019; Smith-Dijak et al., 2019), suggesting it may be a key cellular mechanism mediating circuit dysfunction. Though the normal function of the PNKD protein is unknown, it is located at synapses and appears to participate in regulation of synaptic release *in vitro* (Y. Shen et al., 2015). In the context of either increased excitatory input (stress) or adenosine antagonism (caffeine), iMSNs expressing mutant PNKD protein may have a lower threshold for LTD induction, perhaps by amplification of normal postsynaptic signaling pathways or presynaptic endocannabinoid signaling.

Finally, we observed that, in PNKD mice, manipulations of endocannabinoid signaling could bidirectionally regulate dyskinesia. Pretreatment with the endocannabinoid antagonist AM251 could blunt caffeine-induced changes in iMSN firing rates, as well as dyskinetic attacks. These results suggest that endocannabinoid signaling is required to trigger the profound decreases in iMSN firing that resulted from caffeine treatment and, moreover, that CB1 signaling is required for dyskinesia. Our slice physiology experiments, which focused exclusively on excitatory inputs onto MSNs, suggest that AM251 may prevent the reduction in iMSN firing rates and the induction of dyskinesia by blocking striatal LTD. We also found that the MAGL inhibitor JZL184, which would be predicted to potentiate 2-AG (Long et al., 2009), the endocannabinoid species generated by A2a receptor antagonist treatment (Lerner et al., 2010), lowered the threshold for caffeine-induced dyskinetic attacks *in vivo*. *In vivo*, JZL-184 has been reported to have a number of different dose-dependent behavioral effects, including reducing pain responses, social behavior, increasing motivated behaviors, and interestingly, reducing locomotor activity (Long et al., 2009; Covey et al., 2018; Folkes et al., 2020). JZL184 has also been shown to promote striatal LTD in *ex vivo* whole-cell recordings in a mouse model of Huntington's disease (Sepers et al., 2018), providing a potential link between endocannabinoid signaling, LTD, and dyskinesia in PNKD. However, endocannabinoid signaling regulates the strength and long-term plasticity of other striatal synapses, including glutamatergic synapses onto striatal interneurons (Manz et al., 2020), local inhibitory synapses deriving from GABAergic interneurons and from other MSNs (Freiman et al., 2006; Adermark et al., 2009; Mathur and Lovinger, 2012). Endocannabinoid signaling also regulates striatal dopamine release (Covey et al., 2017). It is thus possible that the *in vivo* effects of cannabinoid drugs on behavior in PNKD involve dopamine signaling and/or striatal inhibitory transmission, in addition to excitatory inputs onto iMSNs.

Together, these findings highlight a key role for the striatal indirect pathway and synaptic plasticity in the development of dyskinesia episodes in PNKD. While studies in other animal models have stressed the potential importance of the direct pathway (Cenci et al., 1999; Perez et al., 2017), we found that reduced indirect pathway activity may be an alternate physiological correlate, consistent with the idea that the two pathways act in concert to help select appropriate movements, while at the same time suppressing competing movements. Mouse models, such as the one used here, may have limitations in understanding human disorders, but targeting the striatal indirect pathway and endocannabinoid-mediated synaptic plasticity may represent a promising new strategy for the focused treatment of hyperkinetic disorders.

References

Adermark L, Talani G, Lovinger DM (2009) Endocannabinoid-dependent plasticity at GABAergic and glutamatergic synapses in the striatum is regulated by synaptic activity. Eur J Neurosci 29:32–41.

Albanese A, Bhatia K, Bressman SB, Delong MR, Fahn S, Fung VS, Hallett M, Jankovic J, Jinnah HA, Klein C, Lang AE, Mink JW, Teller JK (2013) Phenomenology and classification of dystonia: a consensus update. Mov Disord 28:863–873.

Albin RL, Young AB, Penney JB (1989) The functional anatomy of basal ganglia disorders. Trends Neurosci 12:366–375.

Alcacer C, Andreoli L, Sebastianutto I, Jakobsson J, Fieblinger T, Cenci MA (2017) Chemogenetic stimulation of striatal projection neurons modulates responses to Parkinson's disease therapy. J Clin Invest 127:720–734.

Avchalumov Y, Volkmann CE, Ruckborn K, Hamann M, Kirschstein T, Richter A, Kohling R (2013) Persistent changes of corticostriatal plasticity in dt(sz) mutant hamsters after age-dependent remission of dystonia. Neuroscience 250:60–69.

Berardelli A, Rothwell JC, Hallett M, Thompson PD, Manfredi M, Marsden CD (1998) The pathophysiology of primary dystonia. Brain 121:1195–1212.

Bock R, Shin JH, Kaplan AR, Dobi A, Markey E, Kramer PF, Gremel CM, Christensen CH, Adrover MF, Alvarez VA (2013) Strengthening the accumbal indirect pathway promotes resilience to compulsive cocaine use. Nat Neurosci 16:632–638.

Borgkvist A, Avegno EM, Wong MY, Kheirbek MA, Sonders MS, Hen R, Sulzer D (2015) Loss of striatonigral GABAergic presynaptic inhibition enables motor sensitization in Parkinsonian mice. Neuron 87:976–988.

Burke DA, Rotstein HG, Alvarez VA (2017) Striatal local circuitry: a new framework for lateral inhibition. Neuron 96:267–284.

Calderon DP, Fremont R, Kraenzlin F, Khodakhah K (2011) The neural substrates of rapid-onset dystonia-parkinsonism. Nat Neurosci 14:357–365.

Cenci MA, Tranberg A, Andersson M, Hilbertson A (1999) Changes in the regional and compartmental distribution of FosB- and JunB-like immunoreactivity induced in the dopamine-denervated rat striatum by acute or chronic L-dopa treatment. Neuroscience 94:515–527.

Cenci MA, Jorntell H, Petersson P (2018) On the neuronal circuitry mediating L-DOPA-induced dyskinesia. J Neural Transm (Vienna) 125:1157–1169.

Chen CH, Fremont R, Arteaga-Bracho EE, Khodakhah K (2014) Short latency cerebellar modulation of the basal ganglia. Nat Neurosci 17:1767–1775.

Chiken S, Shashidharan P, Nambu A (2008) Cortically evoked long-lasting inhibition of pallidal neurons in a transgenic mouse model of dystonia. J Neurosci 28:13967–13977.

Choi S, Lovinger DM (1997a) Decreased frequency but not amplitude of quantal synaptic responses associated with expression of corticostriatal long-term depression. J Neurosci 17:8613–8620.

Choi S, Lovinger DM (1997b) Decreased probability of neurotransmitter release underlies striatal long-term depression and postnatal development of corticostriatal synapses. Proc Natl Acad Sci USA 94:2665–2670.

Covey DP, Mateo Y, Sulzer D, Cheer JF, Lovinger DM (2017) Endocannabinoid modulation of dopamine neurotransmission. Neuropharmacology 124:52–61.

Covey DP, Dantrassy HM, Yohn SE, Castro A, Conn PJ, Mateo Y, Cheer JF (2018) Inhibition of endocannabinoid degradation rectifies motivational and dopaminergic deficits in the Q175 mouse model of Huntington's disease. Neuropsychopharmacology 43:2056–2063.

Cui G, Jun SB, Jin X, Pham MD, Vogel SS, Lovinger DM, Costa RM (2013) Concurrent activation of striatal direct and indirect pathways during action initiation. Nature 494:238–242.

Damier P, Thobois S, Witjas T, Cuny E, Derost P, Raoul S, Mertens P, Peragut JC, Lemaire JJ, Burbaud P, Nguyen JM, Llorca PM, Rascol O, French Stimulation for Tardive Dyskinesia (STARDYS) Study Group (2007) Bilateral deep brain stimulation of the globus pallidus to treat tardive dyskinesia. Arch Gen Psychiatry 64:170–176.

Day M, Wokosin D, Plotkin JL, Tian X, Surmeier DJ (2008) Differential excitability and modulation of striatal medium spiny neuron dendrites. J Neurosci 28:11603–11614.

Dayne Mayfield R, Larson G, Orona RA, Zahniser NR (1996) Opposing actions of adenosine A2a and dopamine D2 receptor activation on GABA release in the basal ganglia: evidence for an A2a/D2 receptor interaction in globus pallidus. Synapse 22:132–138.

Deffains M, Bergman H (2015) Striatal cholinergic interneurons and cortico-striatal synaptic plasticity in health and disease. Mov Disord 30:1014–1025.

DeLong MR (1990) Primate models of movement disorders of basal ganglia origin. Trends Neurosci 13:281–285.

Dobbs LK, Kaplan AR, Lemos JC, Matsui A, Rubinstein M, Alvarez VA (2016) Dopamine regulation of lateral inhibition between striatal neurons gates the stimulant actions of cocaine. Neuron 90:1100–1113.

Doyle JP, Dougherty JD, Heiman M, Schmidt EF, Stevens TR, Ma G, Bupp S, Shrestha P, Shah RD, Doughty ML, Gong S, Greengard P, Heintz N (2008) Application of a translational profiling approach for the comparative analysis of CNS cell types. Cell 135:749–762.

Fieblinger T, Graves SM, Sebel LE, Alcacer C, Plotkin JL, Gertler TS, Chan CS, Heiman M, Greengard P, Cenci MA, Surmeier DJ (2014) Cell type-specific plasticity of striatal projection neurons in parkinsonism and L-DOPA-induced dyskinesia. Nat Commun 5:5316.

Folkes OM, Báldi R, Kondev V, Marcus DJ, Hartley ND, Turner BD, Ayers JK, Baechle JJ, Misra MP, Altemus M, Grueter CA, Grueter BA, Patel S (2020) An endocannabinoid-regulated basolateral amygdala-nucleus accumbens circuit modulates sociability. J Clin Invest 130:1728–1742.

Freiman I, Anton A, Monyer H, Urbanski MJ, Szabo B (2006) Analysis of the effects of cannabinoids on identified synaptic connections in the caudate-putamen by paired recordings in transgenic mice. J Physiol 575:789–806.

Fremont R, Calderon DP, Maleki S, Khodakhah K (2014) Abnormal high-frequency burst firing of cerebellar neurons in rapid-onset dystonia-parkinsonism. J Neurosci 34:11723–11732.

Gage GJ, Stoetzner CR, Wiltschko AB, Berke JD (2010) Selective activation of striatal fast-spiking interneurons during choice execution. Neuron 67:466–479.

Gerdeman GL, Ronesi J, Lovinger DM (2002) Postsynaptic endocannabinoid release is critical to long-term depression in the striatum. Nat Neurosci 5:446–451.

Gerfen CR, Paletzki R, Heintz N (2013) GENSAT BAC cre-recombinase driver lines to study the functional organization of cerebral cortical and basal ganglia circuits. Neuron 80:1368–1383.

Gernert M, Richter A, Loscher W (1999) Alterations in spontaneous single unit activity of striatal subdivisions during ontogenesis in mutant dystonic hamsters. Brain Res 821:277–285.

Ghiglieri V, Campanelli F, Marino G, Natale G, Picconi B, Calabresi P (2019) Corticostriatal synaptic plasticity alterations in the R6/1 transgenic mouse model of Huntington's disease. J Neurosci Res 97:1655–1664.

Girasole AE, Lum MY, Nathaniel D, Bair-Marshall CJ, Guenthner CJ, Luo L, Kreitzer AC, Nelson AB (2018) A subpopulation of striatal neurons mediates levodopa-induced dyskinesia. Neuron 97:787–795.e786.

Gong S, Zheng C, Doughty ML, Losos K, Didkovsky N, Schambra UB, Nowak NJ, Joyner A, Leblanc G, Hatten ME, Heintz N (2003) A gene expression atlas of the central nervous system based on bacterial artificial chromosomes. Nature 425:917–925.

Gong S, Doughty M, Harbaugh CR, Cummins A, Hatten ME, Heintz N, Gerfen CR (2007) Targeting Cre recombinase to specific neuron populations with bacterial artificial chromosome constructs. J Neurosci 27:9817–9823.

Hendrix CM, Vitek JL (2012) Toward a network model of dystonia. Ann NY Acad Sci 1265:46–55.

Hernández LF, Castela I, Ruiz-DeDiego I, Obeso JA, Moratalla R (2017) Striatal activation by optogenetics induces dyskinesias in the 6-hydroxydopamine rat model of Parkinson disease. Mov Disord 32:530–537.

Higley MJ, Sabatini BL (2010) Competitive regulation of synaptic Ca^{2+} influx by D2 dopamine and A2A adenosine receptors. Nat Neurosci 13:958–966.

Jijón-Lorenzo R, Caballero-Florán IH, Recillas-Morales S, Cortés H, Avalos-Fuentes JA, Paz-Bermúdez FJ, Erlij D, Florán B (2018) Presynaptic dopamine D2 receptors modulate [(3)H]GABA release at striatopallidal terminals via activation of PLC→IP3→calcineurin and inhibition of AC→cAMP→PKA signaling cascades. Neuroscience 372:74–86.

Jin X, Tecuapetla F, Costa RM (2014) Basal ganglia subcircuits distinctively encode the parsing and concatenation of action sequences. Nat Neurosci 17:423–430.

Kozorovitskiy Y, Saunders A, Johnson CA, Lowell BB, Sabatini BL (2012) Recurrent network activity drives striatal synaptogenesis. Nature 485:646–650.

Kravitz AV, Owen SF, Kreitzer AC (2013) Optogenetic identification of striatal projection neuron subtypes during in vivo recordings. Brain Res 1511:21–32.

Kreitzer AC, Malenka RC (2007) Endocannabinoid-mediated rescue of striatal LTD and motor deficits in Parkinson's disease models. Nature 445:643–647.

LeDoux MS, Hurst DC, Lorden JF (1998) Single-unit activity of cerebellar nuclear cells in the awake genetically dystonic rat. Neuroscience 86:533–545.

Lee HY, Nakayama J, Xu Y, Fan X, Karouani M, Shen Y, Pothos EN, Hess EJ, Fu YH, Edwards RH, Ptácek LJ (2012) Dopamine dysregulation in a mouse model of paroxysmal nonkinesigenic dyskinesia. J Clin Invest 122:507–518.

Lerner TN, Kreitzer AC (2012) RGS4 is required for dopaminergic control of striatal LTD and susceptibility to parkinsonian motor deficits. Neuron 73:347–359.

Lerner TN, Horne EA, Stella N, Kreitzer AC (2010) Endocannabinoid signaling mediates psychomotor activation by adenosine A2A antagonists. J Neurosci 30:2160–2164.

Liang L, DeLong MR, Papa SM (2008) Inversion of dopamine responses in striatal medium spiny neurons and involuntary movements. J Neurosci 28:7537–7547.

Long JZ, Li W, Booker L, Burston JJ, Kinsey SG, Schlosburg JE, Pavón FJ, Serrano AM, Selley DE, Parsons LH, Lichtman AH, Cravatt BF (2009) Selective blockade of 2-arachidonoylglycerol hydrolysis produces cannabinoid behavioral effects. Nat Chem Biol 5:37–44.

Maltese M, March JR, Bashaw AG, Tritsch NX (2021) Dopamine differentially modulates the size of projection neuron ensembles in the intact and dopamine-depleted striatum. Elife 10:e68041.

Manz KM, Ghose D, Turner BD, Taylor A, Becker J, Grueter CA, Grueter BA (2020) Calcium-permeable AMPA receptors promote endocannabinoid signaling at parvalbumin interneuron synapses in the nucleus accumbens core. Cell Rep 32:107971.

Martella G, Tassone A, Sciamanna G, Platania P, Cuomo D, Viscomi MT, Bonsi P, Cacci E, Biagioni S, Usiello A, Bernardi G, Sharma N, Standaert DG, Pisani A (2009) Impairment of bidirectional synaptic plasticity in the striatum of a mouse model of DYT1 dystonia: role of endogenous acetylcholine. Brain 132:2336–2349.

Mathur BN, Lovinger DM (2012) Endocannabinoid-dopamine interactions in striatal synaptic plasticity. Front Pharmacol 3:66.

Mink JW (1996) The basal ganglia: focused selection and inhibition of competing motor programs. Prog Neurobiol 50:381–425.

Narushima M, Hashimoto K, Kano M (2006) Endocannabinoid-mediated short-term suppression of excitatory synaptic transmission to medium spiny neurons in the striatum. Neurosci Res 54:159–164.

Ohara S, Nakagawa S, Tabata K, Hashimoto T (2001) Hemiballism with hyperglycemia and striatal T1-MRI hyperintensity: an autopsy report. Mov Disord 16:521–525.

Oldenburg IA, Sabatini BL (2015) Antagonistic but not symmetric regulation of primary motor cortex by basal ganglia direct and indirect pathways. Neuron 86:1174–1181.

Papa SM, Desimone R, Fiorani M, Oldfield EH (1999) Internal globus pallidus discharge is nearly suppressed during levodopa-induced dyskinesias. Ann Neurol 46:732–738.

Parker JG, Marshall JD, Ahanonu B, Wu YW, Kim TH, Grewe BF, Zhang Y, Li JZ, Ding JB, Ehlers MD, Schnitzer MJ (2018) Diametric neural ensemble dynamics in parkinsonian and dyskinetic states. Nature 557:177–182.

Perez XA, Zhang D, Bordia T, Quik M (2017) Striatal D1 medium spiny neuron activation induces dyskinesias in parkinsonian mice. Mov Disord 32:538–548.

Picconi B, Centonze D, Hakansson K, Bernardi G, Greengard P, Fisone G, Cenci MA, Calabresi P (2003) Loss of bidirectional striatal synaptic plasticity in L-DOPA-induced dyskinesia. Nat Neurosci 6:501–506.

Picconi B, Passino E, Sgobio C, Bonsi P, Barone I, Ghiglieri V, Pisani A, Bernardi G, Ammassari-Teule M, Calabresi P (2006) Plastic and behavioral abnormalities in experimental Huntington's disease: a crucial role for cholinergic interneurons. Neurobiol Dis 22:143–152.

Planert H, Berger TK, Silberberg G (2013) Membrane properties of striatal direct and indirect pathway neurons in mouse and rat slices and their modulation by dopamine. PLoS One 8:e57054.

Ramirez-Zamora A, Ostrem JL (2018) Globus pallidus interna or subthalamic nucleus deep brain stimulation for Parkinson disease: a review. JAMA Neurol 75:367–372.

Reiner A, Albin RL, Anderson KD, D'Amato CJ, Penney JB, Young AB (1988) Differential loss of striatal projection neurons in Huntington disease. Proc Natl Acad Sci USA 85:5733–5737.

Roseberry TK, Lee AM, Lalive AL, Wilbrecht L, Bonci A, Kreitzer AC (2016) Cell-type-specific control of brainstem locomotor circuits by basal ganglia. Cell 164:526–537.

Ryan MB, Bair-Marshall C, Nelson AB (2018) Aberrant striatal activity in Parkinsonism and levodopa-induced dyskinesia. Cell Rep 23:3438–3446. e3435.

Schiffmann SN, Jacobs O, Vanderhaeghen JJ (1991) Striatal restricted adenosine A2 receptor (RDC8) is expressed by enkephalin but not by substance P neurons: an in situ hybridization histochemistry study. J Neurochem 57:1062–1067.

Schrock LE, Ostrem JL, Turner RS, Shimamoto SA, Starr PA (2009) The subthalamic nucleus in primary dystonia: single-unit discharge characteristics. J Neurophysiol 102:3740–3752.

Sepers MD, Smith-Dijak A, LeDue J, Kolodziejczyk K, Mackie K, Raymond LA (2018) Endocannabinoid-specific impairment in synaptic plasticity in striatum of Huntington's disease mouse model. J Neurosci 38:544–554.

Sethi KD, Nichols FT, Yaghmai F (1987) Generalized chorea due to basal ganglia lacunar infarcts. Mov Disord 2:61–66.

Shakkottai VG, Batla A, Bhatia K, Dauer WT, Dresel C, Niethammer M, Eidelberg D, Raike RS, Smith Y, Jinnah HA, Hess EJ, Meunier S, Hallett M, Fremont R, Khodakhah K, LeDoux MS, Popa T, Gallea C, Lehericy S, Bostan AC, et al. (2017) Current opinions and areas of consensus on the role of the cerebellum in dystonia. Cerebellum 16:577–594.

Shen W, Flajolet M, Greengard P, Surmeier DJ (2008) Dichotomous dopaminergic control of striatal synaptic plasticity. Science 321:848–851.

Shen Y, Lee HY, Rawson J, Ojha S, Babbitt P, Fu YH, Ptacek LJ (2011) Mutations in PNKD causing paroxysmal dyskinesia alters protein cleavage and stability. Hum Mol Genet 20:2322–2332.

Shen Y, Ge WP, Li Y, Hirano A, Lee HY, Rohlmann A, Missler M, Tsien RW, Jan LY, Fu YH, Ptáček LJ (2015) Protein mutated in paroxysmal dyskinesia interacts with the active zone protein RIM and suppresses synaptic vesicle exocytosis. Proc Natl Acad Sci USA 112:2935–2941.

Shuen JA, Chen M, Gloss B, Calakos N (2008) Drd1a-tdTomato BAC transgenic mice for simultaneous visualization of medium spiny neurons in the direct and indirect pathways of the basal ganglia. J Neurosci 28:2681–2685.

Smith Y, Bevan MD, Shink E, Bolam JP (1998) Microcircuitry of the direct and indirect pathways of the basal ganglia. Neuroscience 86:353–387.

Smith-Dijak AI, Sepers MD, Raymond LA (2019) Alterations in synaptic function and plasticity in Huntington disease. J Neurochem 150:346–365.

Stachniak TJ, Ghosh A, Sternson SM (2014) Chemogenetic synaptic silencing of neural circuits localizes a hypothalamus→midbrain pathway for feeding behavior. Neuron 82:797–808.

Standaert DG (2011) Update on the pathology of dystonia. Neurobiol Dis 42:148–151.

Taverna S, Ilijic E, Surmeier DJ (2008) Recurrent collateral connections of striatal medium spiny neurons are disrupted in models of Parkinson's disease. J Neurosci 28:5504–5512.

Tecuapetla F, Koos T, Tepper JM, Kabbani N, Yeckel MF (2009) Differential dopaminergic modulation of neostriatal synaptic connections of striatopallidal axon collaterals. J Neurosci 29:8977–8990.

Tecuapetla F, Matias S, Dugue GP, Mainen ZF, Costa RM (2014) Balanced activity in basal ganglia projection pathways is critical for contraversive movements. Nat Commun 5:4315.

Tecuapetla F, Jin X, Lima SQ, Costa RM (2016) Complementary contributions of striatal projection pathways to action initiation and execution. Cell 166:703–715.

Washburn S, Fremont R, Moreno-Escobar MC, Angueyra C, Khodakhah K (2019) Acute cerebellar knockdown of Sgce reproduces salient features of myoclonus-dystonia (DYT11) in mice. Elife 8:e52101.

Wei W, Ding S, Zhou FM (2017) Dopaminergic treatment weakens medium spiny neuron collateral inhibition in the parkinsonian striatum. J Neurophysiol 117:987–999.

Wei W, Li L, Yu G, Ding S, Li C, Zhou FM (2013) Supersensitive presynaptic dopamine D2 receptor inhibition of the striatopallidal projection in nigrostriatal dopamine-deficient mice. J Neurophysiol 110:2203–2216.